Elements of the Microphysical Structure of Numerically Simulated Nonprecipitating Stratocumulus

BJORN STEVENS

Department of Atmospheric Science, Colorado State University, Fort Collins, Colorado

GRAHAM FEINGOLD

Cooperative Institute for Research in the Atmosphere, Colorado State University, Fort Collins, Colorado

WILLIAM R. COTTON AND ROBERT L. WALKO

Department of Atmospheric Science, Colorado State University, Fort Collins, Colorado

(Manuscript received 8 May 1995, in final form 3 October 1995)

ABSTRACT

A set of 500 simulated trajectories and a simple parcel model are used to (i) evaluate the performance of a large eddy simulation model coupled to a detailed representation of the droplet spectrum (the LES-BM model) and (ii) gain insight into the microphysical structure of numerically simulated nonprecipitating stratocumulus. The LES-BM model reasonably reproduces many observed features of stratocumulus. The largest sources of error appear to be associated with limited vertical resolution, the neglect of gas kinetic effects and the inability of the model to properly represent mixing across cloud interfacial boundaries. The first two problems have simple remedies; for instance, a condensation–nucleation scheme is derived that includes gas–kinetic effects thus obviating the second problem. The third source of error poses a more vexing, and as yet unsolved, problem for models of the class described herein.

Trajectory timescales are analyzed and in-cloud residence times are found to be, in the mean, on the order of the large eddy turnover time. In addition, it is shown that the length of time trajectories spend near cloud top may be an important factor in the droplet growth equation for a certain favored subset of trajectories. An analysis of the adiabatic trajectory data also indicates that (i) values of diameter dispersion are a factor of 2 to 5 smaller than commonly observed; (ii) simulated values of the dispersion in number concentration are found to be explainable solely on the basis of trajectories having different updraft velocities; (iii) diameter dispersions are not found to be equal to a third of number dispersions, nor did they relate simply to the dispersion in the cloud-base updraft velocity.

Problems with coupling one- and two-dimensional models to detailed representations of the droplet spectrum are discussed. In the case of the former, the lack of an explicit representation of turbulent eddies requires that the coupling between the microphysics and the dynamics be parameterized. In the case of the latter, boundary layer eddies are represented, thus allowing for a more reasonable coupling between turbulence and microphysics. However, the resolved eddies have a different structure than their three-dimensional counterparts, one consequence of which is that timescales of in-cloud circulations are found to be shorter and have less variability.

1. Introduction

Over the past decade or so the evolution and equilibria of persistent decks of stratocumulus climatologically clinging to the edge of summertime subtropical highs has been an issue of increased scientific inquiry. The particular interest in the microphysical structure of these clouds stems from a variety of hypotheses that suggest that anthropogenic influences or biogenic feedbacks may alter their radiative properties in a climatically significant manner. Among the hypotheses that have received wide attention are those of Twomey (1977), Albrecht (1989), and Baker and Charlson (1990); although more recent hypotheses formulated by Pincus and Baker (1994) and Ackerman et al. (1993) are also of interest.

Each of these hypotheses is fundamentally coupled to the evolution of the droplet spectra. Consequently, their detailed consideration through the use of numerical simulations requires that both the droplet distribution function and its interaction with the aerosol distribution function be properly represented. Over the course of the past few years, two groups [e.g., The University of Oklahoma group (Kogan et al. 1994) and the Colorado State University group (Feingold et al.

Corresponding author address: Bjorn Stevens, Dept. of Atmospheric Science, Colorado State University, Fort Collins, CO 80523.
E-mail: stevens@spot.atmos.colostate.edu

1994)] have begun to address this requirement by fully representing the turbulent evolution of the boundary layer via a large eddy simulation (LES) representation of the dynamics coupled to a sectional or binned (BM) representation of the droplet spectrum microphysics (hereafter, the model that results from such a coupling will be referred to as an LES-BM model). The advantage of such an approach is that it provides a consistent representation of the evolution of the cloud dynamical and microphysical structure. Its major drawback is that in order to capture even the most rudimentary interactions between drops and ambient aerosol (e.g., cloud-drop activation) several million degrees of freedom, which represent processes active on time and spatial scales that span several orders of magnitude, must be represented. Consequently, a critical assessment of a model that posits itself as an analog to nature at this level of complexity is an important, yet daunting task.

Perhaps for this reason, earlier reports on simulations of the kind to be reported here left considerable room for further critical assessment. For instance, while Kogan et al. (1994) were the first to present spectrum-resolving simulations of stratocumulus in three spatial dimensions, their simulations were unable to represent the classical feature of number concentrations constant with height, and nonmonotonic operators caused oscillations in prognostic fields near sharp gradients. Feingold et al. (1994) concurrently presented two-dimensional simulations with droplet spectrum resolving microphysics; however, they also experienced problems associated with nonmonotonic numerical operators for advection. As both groups were interested in examining particular sensitivities of their models, only cursory attention was paid to these shortcomings. More recently, Ackerman et al. (1995) presented detailed representations of cloud microstructure generated by coupling a higher-order turbulence closure model to a detailed bin-resolving microphysical model. In comparing their results to observations they were also unable to reproduce the commonly observed feature of constant in height cloud-droplet concentrations. In addition, simulated drizzle rates were compared to only a single observational data point and were obtained on the basis of an aerosol distribution that was not independently initialized. Given this situation, and the recent trend toward using the output of simulations of this class as synthetic datasets for calibrating simpler models, it was felt that there was a need for a more critical assessment of the performance of spectrum-resolving microphysical simulations of marine stratocumulus.

The plethora of observational data that has become available since Nicholls (1989) motivated his work by noting the lack of observational constraints on LES models with grid scales of order 10 m, makes it appealing to attempt to simulate an actually observed case—and assess the model performance based on a detailed comparison to a particular set of observations. Unfortunately, a number of outstanding issues may still make it difficult for the observations to adequately constrain the models. First, is the pervasiveness of specific gaps in the datasets, for example, insufficient observations of subsidence, downward radiative fluxes at cloud top, and the spectrum of cloud condensation nuclei, all of which the model is sensitive to. Second, even in the most recent observations there exists significant (i.e., large enough to make it difficult to adequately constrain the models) uncertainty in concurrent measurements of liquid-water, vapor, and temperature in clouds. Finally, there is the fact that most observations are of physically complex systems, which are affected by a variety of processes, making it difficult to establish fundamental physical relationships. Notwithstanding that simulations of the full physical system are ultimately desired, demonstrating that the model adequately simulates a critical subset of physical processes is a necessary first step. Consequently, while attempts to overcome the obstacles to meaningful observational comparisons [the work of Kogan et al. (1995) being a first step in this regard] are encouraged, the current study takes the alternate approach of simulating a highly idealized case (no shear, no drizzle or collection, no solar radiation). This restricts us to an assessment of the behavior of the model only in the context of observational features that are neither case specific nor strongly dependent on unsimulated processes.

Limiting ourselves to a more qualitative comparison with the observations allows considerable room for error, and develops little new understanding. Consequently, after showing that the model reproduces the classical microphysical features of observed stratocumulus-topped mixed layers, the bulk of this paper is directed to the following two questions: (i) What is the quantitative impact of various assumptions in the model on the simulated microphysical structure of the cloud? (ii) What processes are responsible for producing robust features of the simulated stratocumulus microphysics? Given the implicit assumption that associates robust (in the sense of the numerics) features of the simulations to the actual physical system, the latter question offers the possibility of developing physical insight.

To address these questions a new approach has been developed. This approach is schematically represented in Fig. 1. Here, the LES-BM model is used to generate two sets of information. The first is the structure of an ensemble of trajectories that characterize the boundary-layer circulations. The second is the microphysical structure of the cloud as predicted by the LES-BM model. The ensemble of trajectories is then used to drive a parcel model with different degrees of complexity in the representation of the microphysics (hereafter this model will be referred to as the trajectory ensemble model or TEM). To the extent that the ensemble of trajectories dynamically characterizes the simulated cloud, the microphysical structures predicted by the different models can be compared so as to isolate

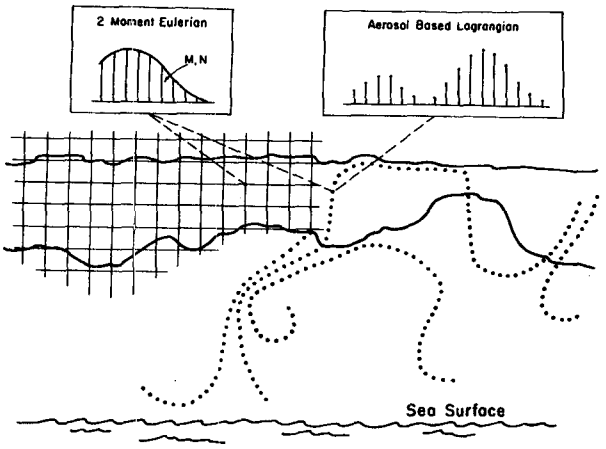

FIG. 1. Schematic representation of different modeling approaches.

the impact of a variety of model assumptions. In the case of the second question, by modifying the structure of the ensemble of trajectories, the manner in which different physical processes contribute to robust features of the *simulated* stratocumulus microstructure is investigated. Moreover, the availability of the trajectory data offers us a different way to consider the cloud and allows us to garner physical insight. Using the trajectory data, the relevant timescales for different processes may be considered, and the manner in which variant trajectories contribute to the inhomogeneity in cloud microstructure can be explored. An analysis of these trajectories, for instance, shows that although much of the mean structure can be reproduced by a single prototypical trajectory, the variance structure depends on the variety of trajectories that constitute the cloud at a given level.

The remainder of the material is organized as follows: sections 2 and 3 describe the LES-BM model and results from the LES-BM simulations, respectively. In section 4 the TEM model is presented. The analysis of the TEM data and its comparison to the LES-BM results is given in section 5. A discussion follows in section 6. The conclusions are summarized in section 7.

2. The LES and LES-BM models

The main modeling component is an LES model that is characterized by an Eulerian representation of physical space and a grid scale in the inertial range of three-dimensional turbulence. Although the model is based on the dynamical framework provided by the Regional Atmospheric Modeling System (Pielke et al. 1992), it contains many new features critical to the current investigations. One such feature is the option of representing the microphysics in the bulk sense or through a detailed representation of the droplet spectrum and its forcings. An overview of the LES and LES-BM models is given below.

a. The dynamical framework

In formulating a limited resolution Eulerian model the equations of motion must first be filtered so that values defined at grid points are representative of grid boxes. Our approach follows Mason (1994), who assumes an unspecified filter implicitly determined by the nature of the subfilter parameterizations. Accordingly, filtered (or grid scale) variables are denoted by an overbar. Such an approach yields a set of equations that may be divided into three categories.

First, is the anelastic momentum equation for a rotating fluid. In the high Reynolds number limit, viscous forces are considered negligible:

$$\frac{\partial \bar{u}_i}{\partial t} = -\bar{u}_j \frac{\partial \bar{u}_i}{\partial x_j} - \theta_0 \frac{\partial \bar{\pi}_1}{\partial x_i} + \frac{g\bar{\theta}_{v1}}{\theta_0}\delta_{i3} + \epsilon_{ijk}(\bar{u}_j - u_{jg})f_k + \frac{1}{\rho_0}\frac{\partial(\rho_0 \tau_{ij})}{\partial x_j}, \quad (1)$$

where the Exner function, π, formulation is used in place of pressure since it simplifies treatment of the buoyancy term. The basic state is given by (π_0, θ_0, ρ_0, u_g, v_g), and is chosen to be in hydrostatic as well as geostrophic balance and to satisfy the ideal gas law for a dry atmosphere. Thermodynamic perturbations from this basic state are denoted by subscript "1."

The subfilter contributions to the filter-scale motions are represented through the term involving the subfilter stress τ_{ij}, where formally, under the as yet unspecified filtering operation, τ_{ij} is defined through the relation

$$\frac{1}{\rho_0}\frac{\partial(\rho_0 \tau_{ij})}{\partial x_j} \equiv \overline{u_j \frac{\partial u_i}{\partial x_j}} - \bar{u}_j \frac{\partial \bar{u}_i}{\partial x_j}. \quad (2)$$

Lilly's stability modification to Smagorinsky's eddy diffusivity method is used for parametrically representing τ_{ij} (Lilly 1962):

$$\tau_{ij} = KD_{ij} \quad \text{where}$$

$$K = l_0^2 \left(\frac{1}{2} D_{ij} D_{kl} \delta_{ik} \delta_{jl}\right) \sqrt{1 - \mathrm{Pr}^{-1}\,\mathrm{Ri}}, \quad (3)$$

where the deformation D_{ij} is given by the traceless form,

$$D_{ij} \equiv \left(\frac{\partial \bar{u}_i}{\partial x_j} + \frac{\partial \bar{u}_j}{\partial x_i} - \frac{2}{3}\delta_{ij}\frac{\partial \bar{u}_k}{\partial x_k}\right), \quad (4)$$

Ri is a gradient Richardson number, Pr is an eddy Prandlt number specified to be 1/3, and $l_0 = 0.25\Delta x$ is an isotropic mixing length scale. This choice of mixing length scales is thought to be equivalent to choosing a filter scale to be on the order of the model's grid scale (e.g., Mason 1994). Nieuwstadt et al. (1991) and Mason (1994) demonstrate the effectiveness of this approach in treating subfilter covariances, and regardless, a verifiable premise of the LES approach is that it is

insensitive to minor details in the subfilter parameterization.

Second, is the equation for the perturbation Exner function, $\bar{\pi}_1$, which follows Klemp and Wilhelmson (1978):

$$\frac{\partial \bar{\pi}_1}{\partial t} = -\left(\frac{R\pi_0}{c_v \rho_0 \theta_0}\right) \frac{\partial(\rho_0 \theta_0 \bar{u}_j)}{\partial x_j}. \quad (5)$$

It is in the sense of this equation that the model is referred to as compressible, although the differences between our model and others in which sound waves are filtered by the incompressibility assumption (e.g., Deardorff 1970; Moeng 1984; Moeng 1986) should be negligible.

Third, is the generalized equation for scalar, $\bar{\psi}$, transport, which is applied to heat, moisture, and microphysical substance transport:

$$\frac{\partial \bar{\psi}}{\partial t} = -\bar{u}_j \frac{\partial \bar{\psi}}{\partial x_j} + \frac{1}{\rho_0} \frac{\partial(\rho_0 \gamma_j)}{\partial x_j} + \mathcal{S}(\bar{\psi}) + [\overline{\mathcal{S}(\psi)} - \mathcal{S}(\bar{\psi})], \quad (6)$$

where $\bar{\psi} \in \{\bar{\theta}_l, \bar{q}_T, \mathcal{M}\}$. Liquid-water potential temperature, $\bar{\theta}_l$, (Betts 1973) and total water, $\bar{q}_T$, are the primary thermodynamic variables. The set of secondary thermodynamic variables (e.g., the microphysical variables) is denoted by $\mathcal{M}$, and will depend on the microphysical representation being used. When $\mathcal{M}$ is empty the model is the standard LES model with "all or nothing condensation," where all the vapor in excess of supersaturation is diagnosed as cloud water. Otherwise the model will have a binned spectrum microphysics representation (thereby fitting our definition of the LES-BM model) where $\mathcal{M}$ will have of order 50 elements, which are described along with their forcings in section 2c below.

Analogous to the definition of τ_{ij} in the momentum equation, γ_j represents the parameterized subfilter contributions, and is a function of the resolved-scale prognostic variable $\bar{\psi}$:

$$\frac{1}{\rho_0} \frac{\partial(\rho_0 \gamma_j)}{\partial x_j} \equiv \overline{u_j \frac{\partial \psi}{\partial x_j}} - \frac{\bar{u}_j}{\rho_0} \frac{\partial(\rho_0 \bar{\psi})}{\partial x_j},$$

where

$$\gamma_i = \mathrm{Pr}^{-1} K \frac{\partial \bar{\psi}}{\partial x_j}. \quad (7)$$

Although the first two terms on the right-hand side of Eq. (6) are familiar, the last three terms may not be. They represent the scalar forcings, and are presented in this manner to raise an often overlooked point (e.g., Ackerman et al. 1995; Bott et al., 1995). The filtering operation should be applied to the system of equations, not the variables. As a consequence, subfilter correlations will arise in nonlinear terms that would otherwise be absent. In the case of the advection equations, the subfilter term is the well-known divergence of the subfilter stresses (which is modeled as a diffusion term). In the case of the scalar forcings (at least in the presence of a resolved droplet spectrum) the sedimentation, condensation, and collection terms all have subfilter contributions. The subfilter correlation in the nonlinear component of the condensation term has been most widely considered; it amounts to a correlation between subfilter variability in the supersaturation and the droplet distribution function. First discussed by Belyaev (1967), it can be thought of as the affect of subfilter turbulent fluctuations on drop spectral evolution. The general problem of how turbulence influences drop spectral evolution is discussed in some detail by Stepanov (1976). Cooper (1989) looks at a limiting case associated with the assumption of equilibrium supersaturations but crossing drop trajectories. While Clark and Hall (1979) attempt to numerically simulate the affect of small-scale random velocity fluctuations on droplet spectral broadening. In our simulations, where the energy-containing eddies are resolved, the neglect of these terms may be warranted, and amounts to the assumption that there is no net contribution to the resolved scales from subfilter correlations in the forcing terms. However, in models that do not converge to the physical system in the limit of infinite spatial resolution (e.g., higher-order closure models, Ackerman et al., 1995; Bott et al., 1995), such neglect may constitute a significant error.

b. *Scalars and their forcings for the standard LES model*

In this case the simple "all or nothing" condensation schemes are considered, where $\bar{\theta}_l$ and $\bar{q}_T$ are the only prognostic scalar variables other than pressure (i.e., $\mathcal{M}$ is empty). Both are conserved under liquid/vapor phase changes, which leads to reduced gradients across cloud edges and fewer errors in the numerical representation (e.g., Tripoli and Cotton 1981; Grabowski and Smolarkiewicz 1990). Moreover, since drops are considered to move with the air, the long- and shortwave radiative flux divergence is the only thermodynamic forcing, and it acts exclusively on $\bar{\theta}_l$. It is parameterized using the mixed emissivity approach described by Chen and Cotton (1983).

c. *Scalars and their forcings for the LES-BM model*

Alternatively, the evolution of the drop spectra may be resolved through its discretization over a fixed grid in mass space. In the present case this discretization is defined by the sequence of 25 mass intervals $[(x_k, x_{k+1})]_{k=1}^{25}$, where $x_1 = 16^{-12}$g, and $x_k = 2x_{k+1}$. Such a specification leads to a grid that spans the diameter interval D (μm) = (3.125, 1008), which should be sufficient for the numerical representation of drops in stra-

tocumulus clouds. The set $\mathcal{M}$ of secondary thermodynamic variables constitutes the basis of the LES-BM formulation and requires that $\mathcal{M} = \{\bar{M}_1, \cdots, \bar{M}_{25}, \bar{N}_1, \cdots, \bar{N}_{25}\}$ be specified. Given $n(x)dx$, the number concentration of drops in a vanishingly small mass interval, $\{\bar{M}_k, \bar{N}_k\}$ are simply the mass and number-mixing ratio of cloud drops within the kth grid interval:

$$\bar{M}_k = \int_{x_k}^{x_{k+1}} xn(x)dx,$$

and

$$\bar{N}_k = \int_{x_k}^{x_{k+1}} n(x)dx. \tag{8}$$

There are a number of advantages to such an approach. First, Tzivion et al. (1987) demonstrate how the use of two moments facilitates the use of broader bin definitions for stochastic collection calculations while maintaining equal or increased accuracy relative to single-moment schemes that have two or three times the number of bins. Second, at least one of the moments of the distribution is conserved under the important forcings of vapor deposition and stochastic collection, thus providing an accurate check or constraint on the numerical procedures used for integrating these processes. Third, use of two moments allows various measures of size to vary freely within a bin.

1) FORCINGS ON THERMODYNAMIC VARIABLES

In addition to considering the forcings on the additional scalars, for the case $\mathcal{M}$ not empty, the radiative forcing on θ_l associated with the standard LES representation is retained. When the assumption that liquid-water moves with the air is relaxed, θ_l and q_t are no longer materially conserved so the divergence of the net liquid-water flux must be represented as a forcing on these terms.

2) FORCINGS ON THE DROPLET SPECTRUM

The present study is primarily concerned with nucleation and condensation of cloud drops, so the model is idealized through the neglect of stochastic collection, sedimentation and drop breakup. As a result, the only forcings on the droplet spectrum are nucleation and condensation/evaporation. The former is discussed in a separate section below. The latter is solved using the semi-Lagrangian method of Tzivion et al. (1989) for which both radiative and gas kinetic effects are assumed negligible. Because these are not necessarily good assumptions some of their limitations are discussed in section 6.

3) SUPERSATURATIONS

The semi-Lagrangian condensation/evaporation scheme of Tzivion et al. (1989) is formulated as a function of an integral average of the vapor surplus over the time step δt:

$$\tau = C(p, T) \int_t^{t+\delta t} \eta(t)dt,$$

where

$$\eta = q_v - q_s, \tag{9}$$

and consequently requires one to accurately represent the evolution of the surplus vapor, $\eta(t)$, over the course of a time step. Since q_v is the vapor-mixing ratio, and q_s is the saturation-mixing ratio, η/q_s is the supersaturation. Consequently, the solution method for $\eta(t)$ is formally identical to that first presented by Squires (1952, see also Sedunov 1965), and has come to be referred to as the semianalytic method for representing the evolution of some measure of the supersaturation field over a time step (Clark 1973). The present work represents an improvement over previous work (e.g., Tzivion et al. 1989; Feingold et al. 1994) in that dynamical forcings over the course of a time step are now considered in the determination of η.

4) ACTIVATION/REGENERATION

The diagnostic activation scheme is based on the cumulative method discussed by Clark (1974a) where each time step the number of drops in the first size interval are incremented by the factor

$$\Delta N_1 = \max\left[0, \bar{N}_T \int_{r_a}^{\infty} f(r; r_g, \sigma_g)dr - \sum_{k=1}^{25} \bar{N}_k,\right] \tag{10}$$

and the mass in the corresponding size interval is incremented by

$$\Delta M_1 = \alpha \Delta N_1 x_1. \tag{11}$$

The scheme activates all previously unactivated aerosol larger than an activation radius, r_a, determined on the basis of equilibrium theory. The aerosol are assumed to be described by a constant lognormal distribution function characterized by (r_g, σ_g), which represent the mean and standard deviation of $\ln r$, respectively. In accord with the observations of Shettle and Fenn (1979), $r_g = 0.03$ μm, and $\sigma_g = 2.2$ are chosen and held fixed during the course of a simulation. In solving for r_a the chemical composition of the aerosol must be specified. Here it is taken to be ammonium bisulphate with a practical osmotic coefficient of 0.9. Here $\bar{N}_T$ is the local aerosol concentration. The sum of cloud drops, $\Sigma \bar{N}_k$, represents the number of previously activated drops, so that in this scheme regeneration is implicit. The factor α in the relation describing ΔM_1 attempts to compensate for the fact that aerosol will not necessarily grow, upon activation, to the size of the smallest bin; it is taken to be the smallest number in

the interval [1/4, 1], which maintains the average mass within the bin.

The current approach (which behaves perfectly in the absence of nonconservative forcings on the aerosol spectrum) represents a departure from previous work. Feingold et al. (1994) used a scheme based on two lognormal distributions each with three prognostic variables. Feingold et al. (1996) use a six-bin scheme associated with six prognostic aerosol categories. Both schemes regenerate aerosols by assuming that the regenerated aerosol is distributed in a spectrum identical to the globally averaged activation spectrum. The chief limitation of the current method is that it is unable to represent cloud processing of the aerosol by processes (e.g., collection and sedimentation), which are anyway neglected in the current study.

d. Boundary conditions

In the horizontal, boundary conditions are doubly periodic. The model top is a rigid lid. To prevent spurious reflections of gravity waves, a fictitious damping term (with damping timescale $\tau_f = 60$ s) is applied to the momentum equations over the top seven levels of the model (between 1500 and 2300 m). The lower surface is a material surface across which fluxes of heat moisture and momentum are solved following Louis (1979). The roughness length of the lower sea surface is given by Charnock's (1955) relation.

e. Numerical methods

The grid spacing is chosen: $\Delta x = \Delta y = 55$ m. Below 900 m, $\Delta z = 25$ m. Above 900 m the grid is progressively stretched so that grid spacings are $O(100$ m) at the model top, which is at approximately 2300 m. Various time-marching schemes are used in the model; however, all explicit time-marching schemes—apart from the one used to solve for acoustic terms in the Exner function equation—operate on a long time step of $\delta t = 2$ s. Radiation calculations are done every five time steps (or 10 s), although heating/cooling rates are applied at each time step. In the momentum equations, leapfrog time differencing is used for the advective terms, while sound wave terms are time split and integrated on a short time step using a Crank–Nicholson semi-implicit scheme in the vertical. Diffusion terms are integrated implicitly in the vertical and explicitly in the horizontal. Forward time differencing is used for the scalar transport equations, which facilitates the use of nonlinear flux correctors in the representation of scalar advection.

Variables are defined on the Arakawa C-grid for which grid stretching and interactive nesting are available options. The eddy diffusivities are calculated at thermodynamic points and averaged to w points. The nonlinear advection of momentum is computed using fourth-order centered in space differencing. Scalars are advected using sixth-order differencing in space based on the polynomial forms of Tremback et al. (1987) coupled with the flux limiters in order to maintain monotonicity in the solutions. The flux limiters are built according to the FCT methodology of Boris and Book, which is discussed in some detail by Smolarkiewicz and Grabowski (1990) as well as by Zalesak (1979). In our implementation, limiters are constructed as described in Smolarkiewicz and Grabowski (1990) with modifications as per the discussion in Zalesak (1979). All advection schemes are formally one-dimensional and are successively (through the course of a time step) applied to each velocity component in turn.

3. LES-BM results

a. Overview

1) Initialization and spinup

The LES-BM model is initialized as in Moeng et al. (1996) with the exception that above cloud, air is moistened and warmed so as to make the cloud top jump in θ_e positive. Increasing the stability of the cloud-top interface results in unbroken cloud cover (e.g., see Fig. 2). The upper boundary condition in the mixed emmisivity scheme is chosen to give downward longwave fluxes of 240 W m^{-2} at 1000 m. This led to cooling rates on the order of 8 K h^{-1} in the top 25 m of the cloud.

The model is spun up with the simple (and much faster) saturation adjustment scheme. After about 60 min of simulation time it reaches a quasi-steady state where fluxes of conserved variables (not shown) are determined to be linear with height and the turbulence field varies slowly (see TKE in Fig. 2). At 90 min a BM run is spawned, within which trajectories are computed. The mapping of the diagnosed liquid-water field (associated with the standard LES spinup) onto the two-moment Eulerian grid, which tracked drops in the BM run, is done by assuming an activated fraction of aerosol of 0.75, and a lognormal distribution function for the water with standard deviation $\sigma_g = 1.2$. This in turn defines the mean radius of the distribution, allowing it to increase with height in a manner that keeps the number concentration constant. Figure 2 indicates how

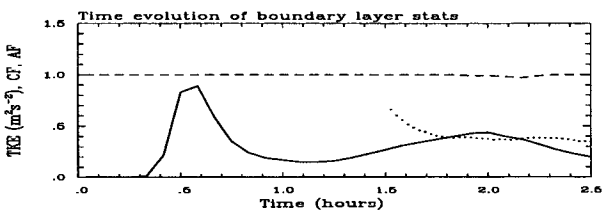

FIG. 2. Time evolution of boundary-layer turbulent statistics. Solid line, boundary layer TKE; dashed line, cloud fraction; dots, activated fraction of aerosol.

in about two eddy turnover times (~20 min) the simulated number concentrations equilibrated to a new steady state significantly lower than the initialization.

Because the ability of the model to accurately represent first- and second-order turbulent statistics is demonstrated by Moeng et al. (1996), it shall not be redemonstrated at this point. Notwithstanding, snapshots of flow structures at 150 min are illustrative and are discussed below. Section 3b presents the analysis of the microphysical fields in the BM run, which is based on the final 40 min of the 60-min sensitivity run—as is the TEM analysis.

2) SNAPSHOTS OF FIELDS

Figure 3 demonstrates the cellular cloud features typically associated with stratocumulus. The LWP (liquid-water path) varies by about a factor of 4 or 5 over the domain, with the most pronounced minimum in the northwest corner. Minima in the LWP tend to be narrower than maxima. The collocation of LWP minima and downdrafts indicates that the downdrafts are associated with breaks in the clouds. Near cloud top (e.g., the w field at 700 m in Fig. 4b), the vertical velocity field shows evidence of highly organized downdrafts that define the cellular structure of the cloud. Comparing the cloud-top velocity field (Fig. 4b) with that just below cloud base (Fig. 4a), it is apparent that not all of the downdrafts mix through the depth of the boundary layer. Generally, it is only in the regions of the greatest confluence—such as the corners of the cells defined by the downdrafts—where downdrafts penetrate significantly below cloud base. This observation is supported by an examination of the w field at 300 m, although the figure is not shown.

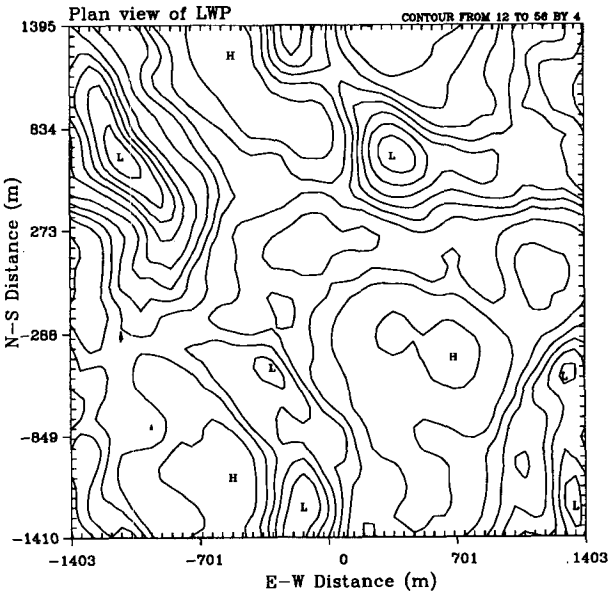

FIG. 3. Vertically integrated liquid-water path. Note that in all contour plots the contour interval and range is given on the top left of plot. Local highs and lows are marked on the plots.

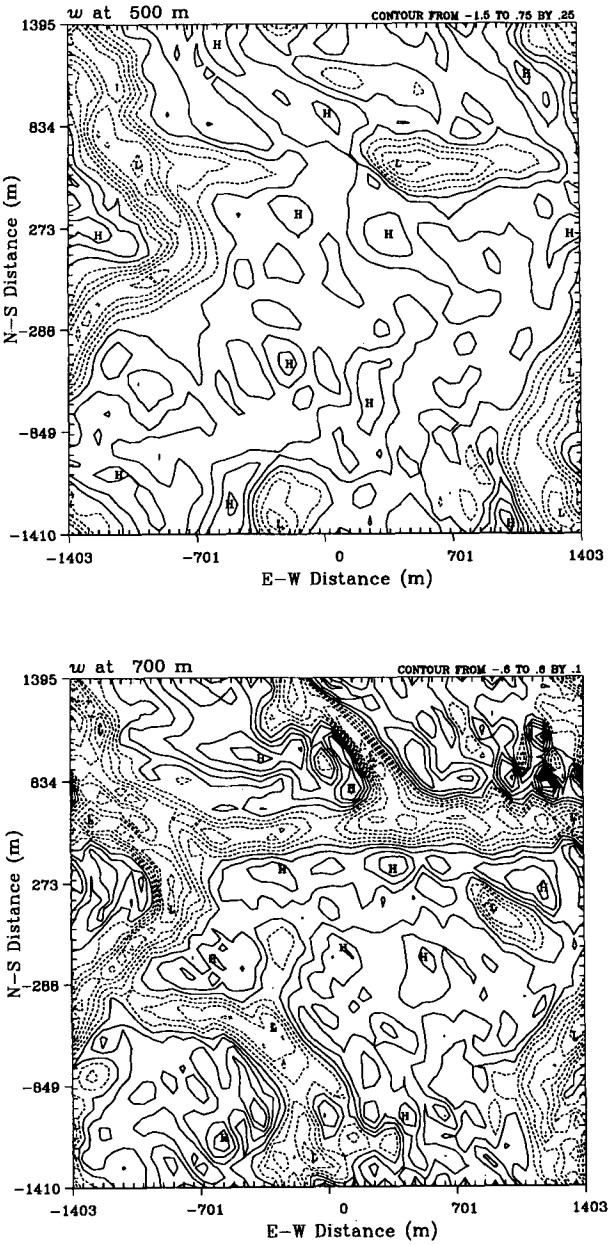

FIG. 4. Vertical velocity field at two different levels: (a) near cloud base z = 500 m, (b) near cloud top z = 700 m.

More evidence of this type of structure is provided by the $x - z$ cross sections taken at $y \approx -1250$ m. The w cross section in Fig. 5a illustrates that while the strongest downdrafts penetrate through the depth of the domain, there exist secondary circulations confined to the cloud layer. Cloud water (Fig. 5b) is greatest in regions of deepest ascent (i.e., where updrafts are most

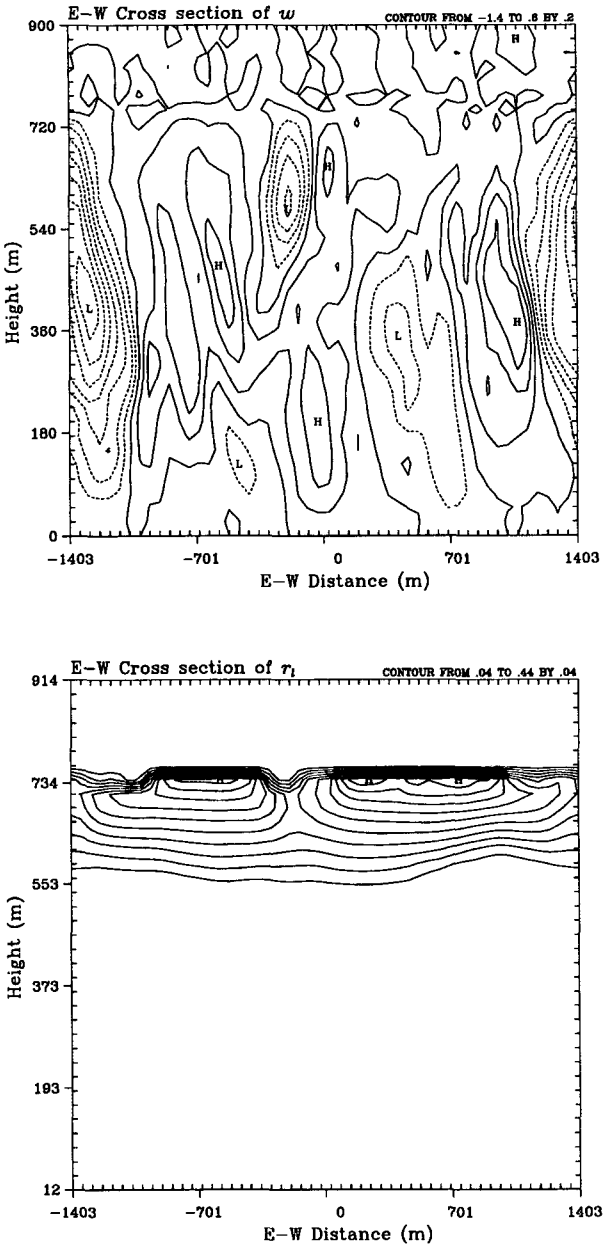

FIG. 5. Cross section of (a) vertical velocities, and (b) associated cross section of liquid-water mixing ratio.

strongly connected to the surface layer), while reliefs of cloud top indicate the collocation of cloud top "valleys" with downdrafts. The supersaturation fields (Fig. 6a) produced by the model appear quite reasonable in that they have well-defined cloud-base maxima of order 0.4%, and fall off through the depth of the cloud. There are secondary maxima near cloud top (of order 0.3%) that seem to be preferentially located in regions of downdrafts. This somewhat classical picture of the supersaturation [excluding the cloud-top features, which are discussed elsewhere (Stevens et al. 1996)] associated with convective motions leads to the equally classical picture of number concentration fields relatively constant with height through the depth of the cloud (Fig. 6b).

b. *Microphysical statistics*

In this section LES-BM data are averaged before presentation and a number of different types of averaging procedures are used. Time averaging is con-

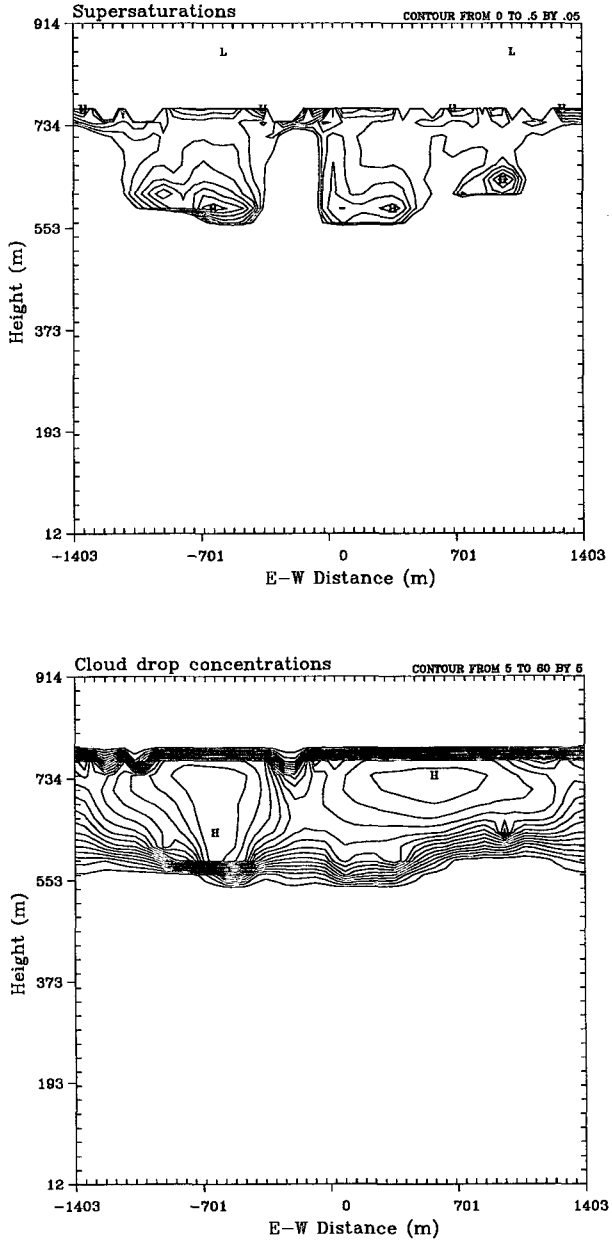

FIG. 6. (a) In-cloud supersaturations, and (b) cloud-drop number concentrations.

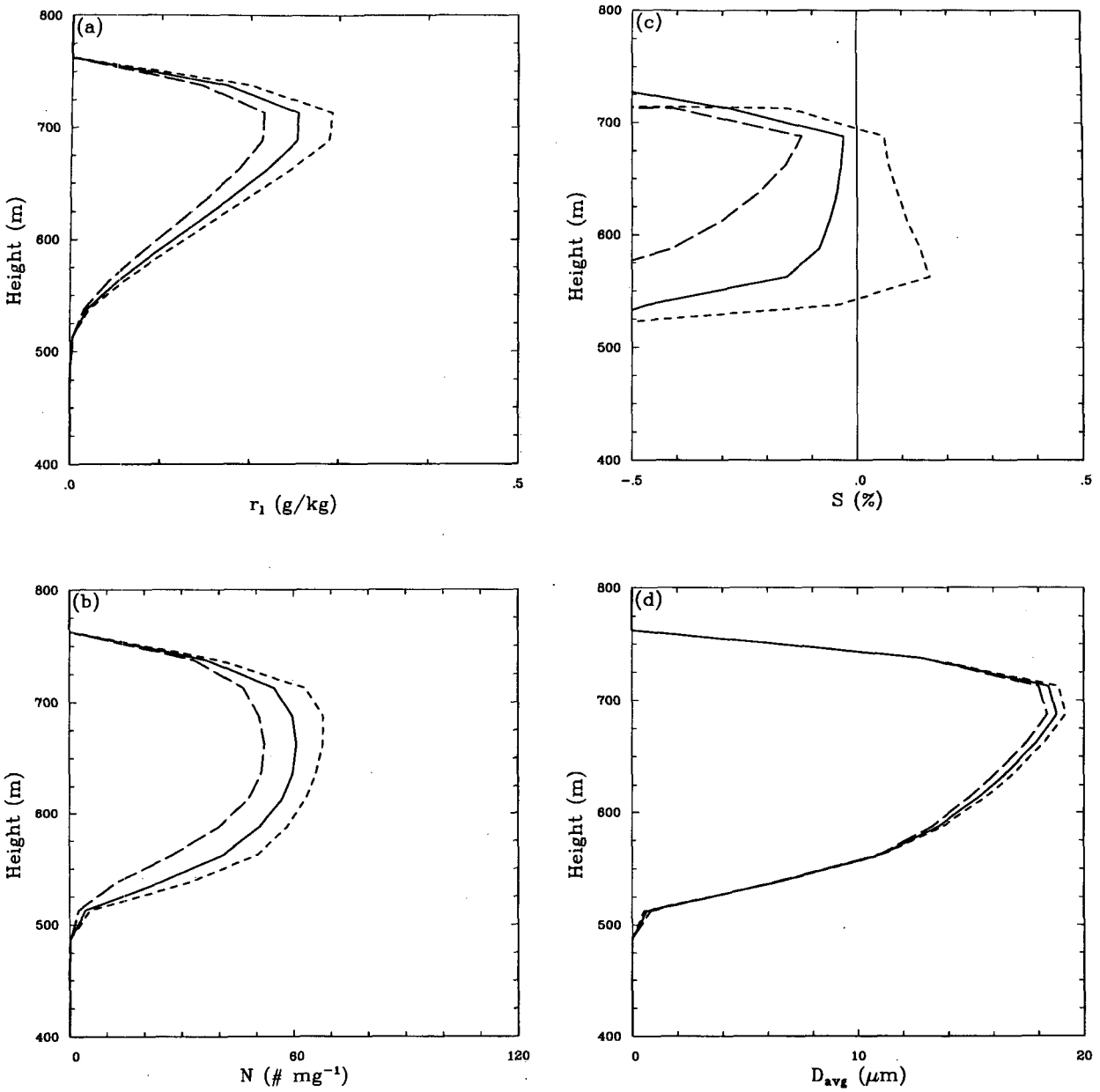

FIG. 7. Mean microphysical profiles: (a) liquid-water mixing ratio; (b) number mixing ratio (units approximately the same as number per cm^{-3}); (c) supersaturation; (d) mean diameters. Layer average (solid line), downdraft average (long dash), updraft average (short dash).

ducted over the nine time levels that span the 40-min analysis period. Space averaging is over the whole domain at a given vertical level. Elements that contribute to an average may be limited through the use of conditional sampling. Two types of conditional sampling are performed; some averages are computed only over up- or downdrafts, whereas other averages are limited to cloudy points. Cloud is defined to exist if a local threshold is satisfied, where for this threshold the liquid-water criterion of 0.02 g kg^{-1} suggested by Noonkester (1984) or a number concentration criterion of 1 cm^{-3} is invoked. The use of two criteria gives us a measure of the robustness of our results with respect to averaging procedures. Unless otherwise stated, all averages are space and time averages.

1) MEAN PROFILES

In Fig. 7 the layer-mean as well as the up/downdraft-mean simulated microphysical structure of the cloud is represented in terms of the liquid-water mixing ratio, number concentration, supersaturation, and

average diameter. Regarding the layer-mean values (solid lines), the cloud drop number concentration curve is approximately constant with height (Fig. 7b), in contrast to the approximately linear increase in liquid water content (Fig. 7a). Such a picture is consistent with activation of cloud drops at cloud base and no subsequent activation through the depth of the cloud. Increases in liquid water content are absorbed by a shifting of the mode diameter on a constant droplet population as evidenced by the increase in average diameter (Fig. 7d) through the depth of the cloud. All of this is in qualitative agreement with the classical[1] picture of nonprecipitating stratocumulus microphysical structure developed on the basis of numerous observations (e.g., Slingo et al. 1982; Noonkester 1984; Nicholls 1984).

The mean supersaturation plotted in Fig. 7c increases with height, but is negative through the depth of the cloud. Conditionally, sampling over up- and downdrafts demonstrates that updrafts are supersaturated in the mean and downdrafts are subsaturated. Using the layer mean supersaturation to couple their higher-order turbulence dynamical representation to their microphysical model, Ackerman et al. (1995) predicted a similar structure in the mean field. Such an approach is in marked contrast to the current model in which the turbulence is resolved and the coupling is through the grid-box averaged supersaturation field. Consequently, although both models predict similar structure in the mean supersaturation, drastically different microphysical structures result, as the present model clearly activates significant numbers of drops in strongly supersaturated updrafts and number concentrations are relatively flat and robust to averaging procedures. These results demonstrate that the important (from the perspective of the microphysics) structure of the supersaturation field is not revealed by the mean, and that the strong correlation between updraft velocity and supersaturation must be accounted for. Another problem with driving microphysical routines with the mean supersaturation is that droplet growth routines will be unable to represent broadening of the drop spectra due to turbulent motions (Cooper 1989).

Supersaturations in clouds are not readily or reliably measured, although they are one of the means by which the dynamics regulates the cloud microphysical structure. Nevertheless, an effective supersaturation may be inferred based on a comparison of cloud drop concentrations and subcloud aerosol activation properties. Using such a procedure for observations of stratocumulus, Hudson and Frisbie (1991) inferred median effective supersaturations between 0.24% and 0.42%. Similarly, Martin et al. (1994) show results that limit cloud-base supersaturations in stratocumulus to $<0.8\%$ with median values of order 0.4%. Consequently, observational inferences about supersaturations are quite consistent with the cloud-base maxima produced by the model (Fig. 6). Moreover, estimating the supersaturations produced in the simulations, using our knowledge of the specified CCN spectra and the mean value of the activated fraction of CCN, an effective cloud-base supersaturation of 0.25%–0.30% is obtained. This is somewhat smaller than the local maxima in Fig. 6 but still consistent with the observational inferences.

Backtracking to the conditionally sampled profiles of liquid water (Fig. 7a), we note that updrafts are considerably moister than downdrafts so that simulated departures from adiabaticity in the mean are largely a function of the quantity of entrained air in the downdrafts. Furthermore, because we are considering layer averages, the presence of dry air in downdrafts at a given level will decrease both the drop concentrations and the liquid water content. This dual effect mitigates the differences between average diameter in up- and downdrafts so that they only differ by about a micrometer (Fig. 7d). The variant properties in the up- and downdrafts tend to contribute to the ragged cloud-base structure ubiquitous in stratocumulus; it is also responsible for smoothing the cloud-edge microphysical profiles so that, for instance, the mean cloud drop concentrations (Fig. 7b) are not as constant with height as they would be in a profile constructed from a single column of grid points at a single time.

2) DISPERSION PROFILES

Observations of microphysical dispersion in stratocumulus (e.g., Noonkester 1984) show the same general character as our simulations (see Fig. 8) where the dispersion in the liquid water, number concentrations, and mean diameter (radius) have maxima at cloud-edges with a single minimum toward the center of the cloud. Although, the cloud-edge maxima tend to be less pronounced in the observations, this is largely a sampling issue, as when we sample according to Noonkester's cloud criteria, the cloud-edge peaks in dispersion are reduced by about a factor of two. Observed minima in the dispersions in number concentration and radius are both slightly under 0.2, although the minimum dispersion in liquid water tends to be larger than 0.2. The simulations develop dispersion minima of about the same order, although simulated diameter dispersions are slightly less, and number dispersions slightly greater than observed. Although relatively large values of diameter dispersion are generated by our model in the absence of collection, given the shallowness of the clouds observed by Noonkester and their large ambient droplet concentrations, it is reasonable to assume that collection contributes little to the values of dispersion he observed.

[1] Although as with most classical features there may be many interesting instances that do not conform to the stereotype.

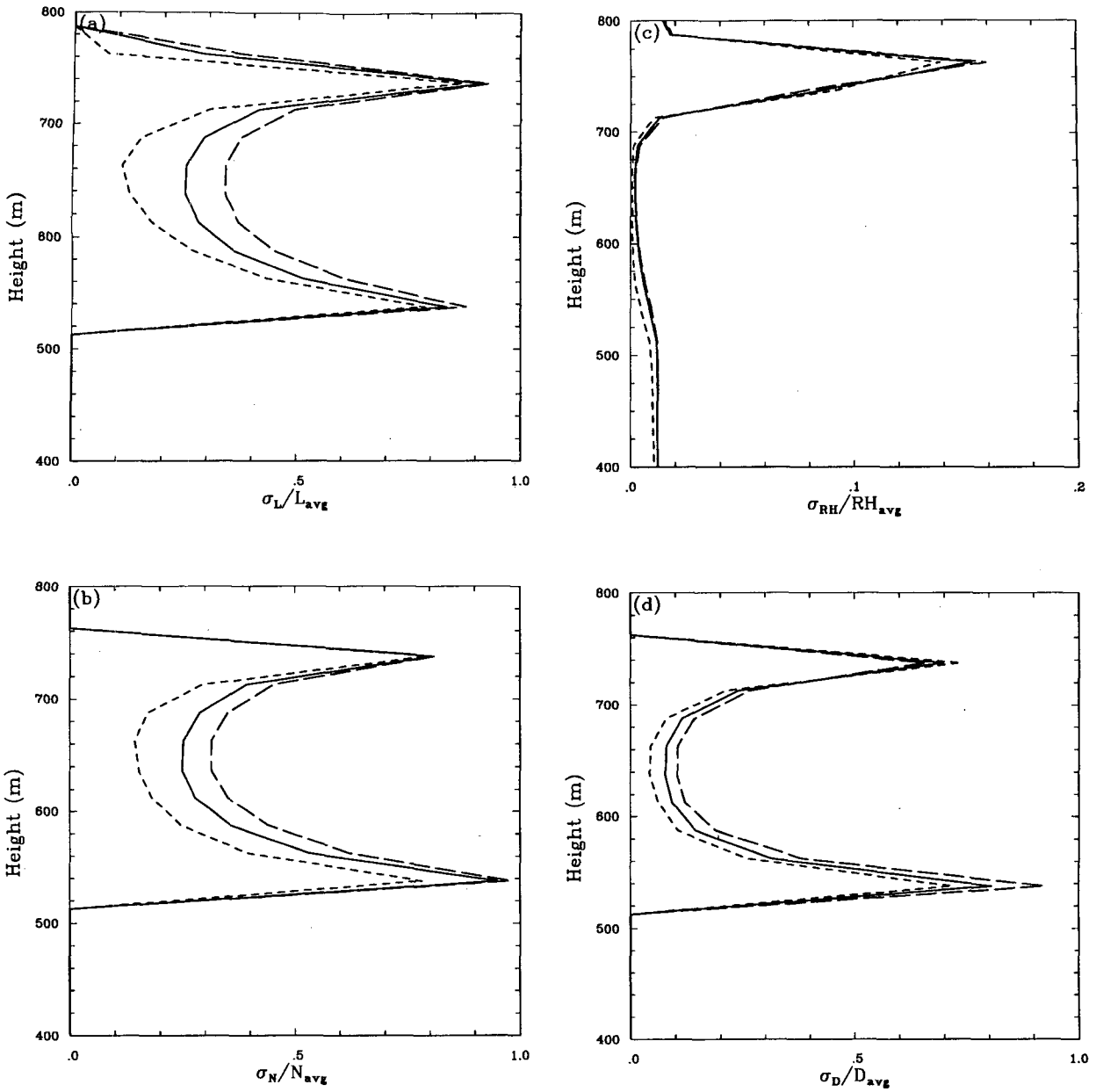

FIG. 8. Microphysical dispersion profiles: (a) liquid-water mixing ratio; (b) number mixing ratio (units approximately the same as number per cm^{-3}); (c) supersaturation; (d) mean diameters. Layer average (solid line), downdraft average (long dash), updraft average (short dash).

In Fig. 8 the dispersion has been partitioned into conditionally sampled values over up- and downdrafts in which the more dispersive nature of the simulated downdrafts is clearly illustrated. Because the dispersion in the downdrafts may be a strong function of the manner in which the model mixes across cloud top, it would be interesting to have conditionally sampled values of actually observed dispersion in order to better assess the realism of the simulations in this regard.

4. The trajectory ensemble model (TEM)

A significant component of the analysis will be based on trajectories derived from the LES model and used to drive the TEM. The TEM can be thought of as a host Lagrangian dynamical framework in which one can embed a variety of microphysical representations. A description of the TEM model, as configured in the context of a Lagrangian representation of the microphysics, is given below. In this section we also discuss

how the TEM represents entrainment, some of its limitations, and the nature of the LES derived trajectory set with which we force it.

a. Model description

For the purposes of this study, the TEM is driven by an ensemble of N trajectories

$$\mathcal{T} = \{T_1, T_2, \cdots, T_N\}.$$

Each trajectory is defined by $T_n \in \mathcal{T}$, which corresponds to a time ordering of, I, 9-dimensional time-history vectors

$$T_n = \{(p_i^n, \theta_{l,i}^n, q_{T,i}^n, x_i^n, y_i^n, z_i^n, u_i^n, v_i^n, w_i^n)\}_{i=1}^{I}$$

that determine the instantaneous thermodynamic state, position, and velocity of the parcel over the course of the nth trajectory. Because, θ_l and q_T are constant in the absence of mixing, their variance is a measure of the entrainment into the parcel. For the present work, the time interval between successive time history vectors is 2 s, over which state variables are assumed to vary linearly.

Trajectories may be prescribed, or predicted by the LES-BM simulations. In the latter case, the LES model predicts the evolution of $\mathcal{T}$, as follows: At the initial time step material elements are distributed randomly in space. At each time level, the values of the state variables, including velocities, are interpolated (trilinearly) from the surrounding grid points to the trajectory's specified position and written to a file. The trajectory's position is then changed according to its velocity and the length of the time step, and the process begins anew. An overview of the LES-derived trajectory set is provided in section 4d below.

The great advantage of the TEM is that its assumptions facilitate a Lagrangian representation of the liquid water mass so that the artificial distinction between drops and aerosols common to Eulerian microphysical models is no longer necessary. By fixing the aerosol sizes, or even binning them, the amount of water mass per aerosol may evolve freely. So from the perspective of the drop spectrum the liquid water is represented in a Lagrangian sense, where drops are treated as delta functions associated with aerosol of differing sizes and differing chemistry. In this context, the evolution of the hygroscopic aerosol may be modeled by a system of ordinary differential equations that can be solved with relative efficiency and arbitrary accuracy through the use of differential equation solvers such as VODE (Brown et al. 1989).

More rigorously, over each time interval and for each trajectory, the following coupled system of K equations for the growth of each cloud drop category is solved:

$$\frac{dr_k}{dt} = g(p, \theta_l, q_T, q_l, r_k; a_k, \beta_k),$$

where

$$q_l = \frac{4}{3}\pi\rho_w \sum n_k (r_k^3 - a_k^3), \tag{12}$$

and $k \in [1, K]$ with K being the number of aerosol categories and n_k being the number mixing ratio in each category. In the present study we take $K = 100$. The function g represents the growth rate of a single drop of wet radius r_k growing on a hygroscopic aerosol described by its dry radius a_k and chemistry parameter β_k under conditions constrained by the present thermodynamic state:

$$g(p, \theta_l, q_T, q_l, r_k; a_k, \beta_k) = \frac{1}{\rho_w r}\left[\frac{q_v - q_r}{\dfrac{1}{\rho_0 D_v^*} + \left(\dfrac{q_r}{q_s}\right)\dfrac{L}{k_a^* T}\left(\dfrac{L}{R_v T} - 1\right)q_s}\right], \tag{13}$$

where temperature T is diagnosed iteratively from the relation

$$\theta_l = \left(\frac{p}{p_0}\right)^{0.286} T \exp\left(\frac{-Lq_l}{C_p T}\right).$$

The vapor mixing ratio q_v is given by $q_T - q_l$. The primary thermodynamic variables p, q_T, and θ_l are given by the time history vector, and are assumed to vary linearly between time levels. The saturation mixing ratio at the drop's surface is modified by the curvature term and the water activity of the solution drop:

$$q_r = q_s \exp[\alpha(T)/r_k - \beta_k(a_k/r_k)^3],$$

where

$$\alpha(T) = \frac{3.298 \times 10^{-5} - 6.717 \times 10^{-8}(T - 273.16)}{T}.$$

Gas kinetic effects are allowed to modify the effective diffusivities for heat and vapor:

$$D_v^* = \frac{D_v}{\dfrac{r}{r + \Delta_v} + \dfrac{D_v}{r\alpha_c}\left(\dfrac{2\pi}{R_v T}\right)^{1/2}}$$

$$k_a^* = \frac{k_a}{\dfrac{r}{r + \Delta_T} + \dfrac{k_a}{r\alpha_T \rho c_p}\left(\dfrac{2\pi}{R_v T}\right)^{1/2}}. \tag{14}$$

The coefficients α_c and α_T are the condensation and thermal accommodation coefficients, respectively, chosen: $\alpha_c = 0.036$, $\alpha_T = 0.7$. The vapor and thermal jump lengths are also fixed at constant values: $\Delta_v = 1.04 \times 10^{-5}$ cm, $\Delta_T = 2.16 \times 10^{-5}$ cm. In addition, c_p is the isobaric specific heat, ρ is the density of the moist air, and R_v is the gas constant for water vapor.

b. Representation of entrainment

For the purposes of the following discussion, entrainment may be thought of in two different senses. Parcel-wise entrainment refers to the mixing of air into parcels defined as neighborhoods about a point that moves with the resolved flow. Layer-wise entrainment refers to the incorporation of free tropospheric air into the boundary layer as part of the process through which the turbulent boundary layer deepens. The model makes a crude attempt at representing the former. The latter is only partially included in that free tropospheric air is mixed across the inversion by trajectories that leave the boundary layer, and then reenter with slightly different thermodynamic properties (instances of this process are considered in the discussion). Parcels of air that wholly originate above the boundary layer are not included in the trajectory set; as we shall see this leads to a slight discrepancy between the TEM-derived liquid water fields relative to the LES-BM analysis.

As discussed earlier, parcel-wise entrainment is represented in terms of a change in the liquid-water potential temperature and total-water mixing ratio. The frequency and magnitude of mixing events is thus determined by how rapidly the thermodynamic state changes along the LES-BM-predicted trajectory. Assuming, as is done here, that parcels immediately take on the properties of their local environment is akin to assuming a mixing timescale of zero. While not warranted, it does represent an interesting limiting case and is simple. Errors from this assumption will be particularly large near cloud top, a point that receives further discussion in section 6a. The current representation of entrainment also assumes that the mixing is homogeneous, so that all the drops feel a uniform change in their local environment due to changes in θ_l and q_T. While this represents an interesting limiting case, mixing is not likely to be so homogeneous; consequently care must be taken in interpreting statistics dependent on mixing events.

c. Limitations of the TEM

In addition, there exist a number of other limitations of the TEM framework: (i) the present formulation allows the parcels to move only as a function of the resolved scale winds. In principle one can add a random velocity component to the resolved scale winds based on the model predicted subgrid TKE (which in our case is an implicit function of the diffusion). However, such a procedure generally assumes isotropy, or an anisotropy derived from that of the resolved scale winds; both assumptions involve considerable amounts of uncertainty. Nevertheless, failure to add a subgrid component to the advecting velocities also has its problems. In particular, trajectories may have a harder time penetrating regions of relatively low resolved-TKE (such as cloud top and near the surface), and caution is warranted in interpreting the trajectory results in these locations (Jeffrey Weil 1995, personal communication). (ii) It is assumed that differences in the microphysics in the TEM simulations will not affect the dynamics in a manner significantly different from what is represented by the LES-BM simulations. Sensitivity tests show that this assumption is justified as the small differences (on the order of the differences between the supersaturations in the LES-BM runs and those in the TEM runs) in the supersaturation fields have virtually no impact on the evolution of the dynamics. (iii) A critical component of the evolution of stratocumulus may depend on what happens at cloud top. Unfortunately the cloud-top dynamics, with their smaller eddies, represent the largest region of uncertainty for the LES. Exactly how the turbulence and radiation interact in this region, and the manner in which entrainment proceeds is only roughly represented by the LES-BM, thereby undermining the credibility of the LES-generated trajectories in the vicinity of cloud top. To the extent that these processes are insensitive to small-scale features of the flow, the LES representation will do a good job. However, if the cloud-top processes are fundamentally related to unresolved processes, the model cannot be expected to accurately simulate reality. These points constitute a central assumption underlying much of the analysis, which the critical reader should bear in mind through the remainder of the discussion.

d. Trajectory structure

An ensemble of 500 trajectories is tracked during the course of the 60-minute LES-BM sensitivity run. Each trajectory is given a random initial position somewhere between the 200- and 450-m levels. Trajectories are initialized below cloud base in order to avoid having to make assumptions about the in-cloud structure of the microphysics in the initialization of the trajectory model.

In Fig. 9, three 60-min trajectories derived from the LES model have been plotted. The trajectories have been chosen from the full ensemble to give a qualitative sense of the range of trajectories one can expect within the turbulent boundary layer; however, none of the trajectories are anomalous. The three trajectories are plotted in different panels as a function of the relative distance from their initial x position. The trajectories travel between 7 and 8.5 km over the 60-min integration, consistent with the ambient wind. The trajectories in the lower two panels are quite similar in some respects. Both gradually rise during the first 20 or so minutes of the simulation, and then undergo a period of gradual descent for the remainder of the simulation. The biggest difference between these two trajectories is that the one in the lowest panel rises through the depth of the cloud, spending a brief period of time in the cloud-top region. The trajectory plotted in the uppermost panel is the most interesting in a number of respects. It rises rapidly

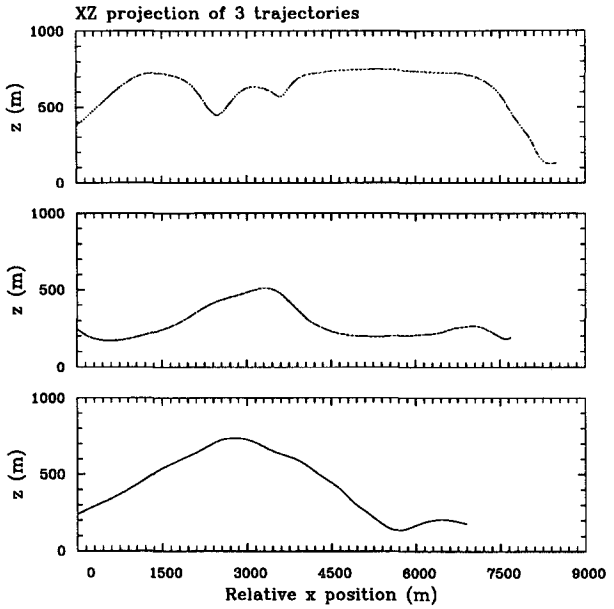

FIG. 9. Sample of evolution of three different types of trajectories over the course of an hour. Cloud base ~ 500 m.

to cloud top and appears to be recycled through the cloud as it is caught in circulations limited to the cloud layer. At one point, however, it becomes confined in the cloud-top region for about 20 min before getting caught in a downdraft that penetrates the depth of the domain and returns it to the lowest level reached by any of the three trajectories considered here. The structure of this trajectory, particularly the length of time it spends in the vicinity of cloud top, would appear to be of some consequence for the microphysical structure of the cloud.

5. TEM analysis

Although the LES-BM fields discussed in this section are the same as presented in section 3, the manner in which the TEM profiles are generated warrants comment. In analyzing the TEM data, trajectories are binned into different 7-m thick layers. Because the average trajectory moved at velocities of order 0.5 m s^{-1}, it can contribute data points to each height bin as it traverses a layer; consequently, there will exist a background variance associated with the binning interval. This background variance associated with the vertical averaging procedure is negligible for most fields, with the exception of the cloud-base liquid water and diameter dispersion (see subsection b). Though one can average over the trajectory segments within a given layer before allowing the trajectory data to contribute to the statistics, the Lagrangian treatment of the droplets makes such a procedure cumbersome. In addition, during the analysis period no regard is paid to the time at which the trajectory reaches a given level, so that a single trajectory can contribute to the statistics at a given level at different times along its evolution. This amounts to an effective time–space average at a given level. LES-BM statistics are computed in the manner described at the top of section 3b and are quite sensitive to the averaging procedure in the lowest 25–50 m of the cloud. When conditional averaging over cloudy points is used, the statistics varied with the sampling threshold. As a result, simple layer averages are used with the implicit understanding that discrepancies near cloud base can largely be explained by the sensitivity to the sampling criteria.

a. Sensitivity to modeling assumptions

To more thoroughly evaluate our results this section discusses the comparisons among the different models. Using the trajectories generated by the LES-BM model to drive the TEM with differing microphysical representations, we first compare the TEM with the LES-BM Eulerian microphysics to the LES-BM data, thereby isolating the impact of the dynamical representation. Next, we compare the TEM data using differing representations of the microphysics, thereby isolating the impact of the various assumptions in the microphysical representation. In all we use the TEM to conduct the four experiments summarized in Table 1. All comparisons are made between statistics computed at a given level. Differences in individual trajectories tend to mirror the differences averaged over a level.

1) EFFECT OF EULERIAN PHYSICAL SPACE REPRESENTATION

The basis of comparison in this section will be between experiment LES-BM and experiment TEM-ENK (TEM with Eulerian microphysics and no kinetic effects). Note that given the different estimates of the liquid-water content, the trajectories do not completely characterize the cloud structure revealed by the layer averages (Fig. 10a). Because liquid water is approximately the difference between two large numbers, the differences between the TEM and LES-BM liquid-water fields can be accounted for by only a 0.1% discrepancy in the prognostic thermodynamic variables (θ_l, q_T). Differences of this order can be accounted for by

TABLE 1. Features of model used to generate data for Figs. 11 and 12.

Experiment name	Dynamical representation	Microphysical representation	Gas kinetic effects?
LES	Eulerian	Eulerian	no
TEM-ENK	Lagrangian	Eulerian	no
TEM-LNK	Lagrangian	Lagrangian	no
TEM-LWK	Lagrangian	Lagrangian	yes

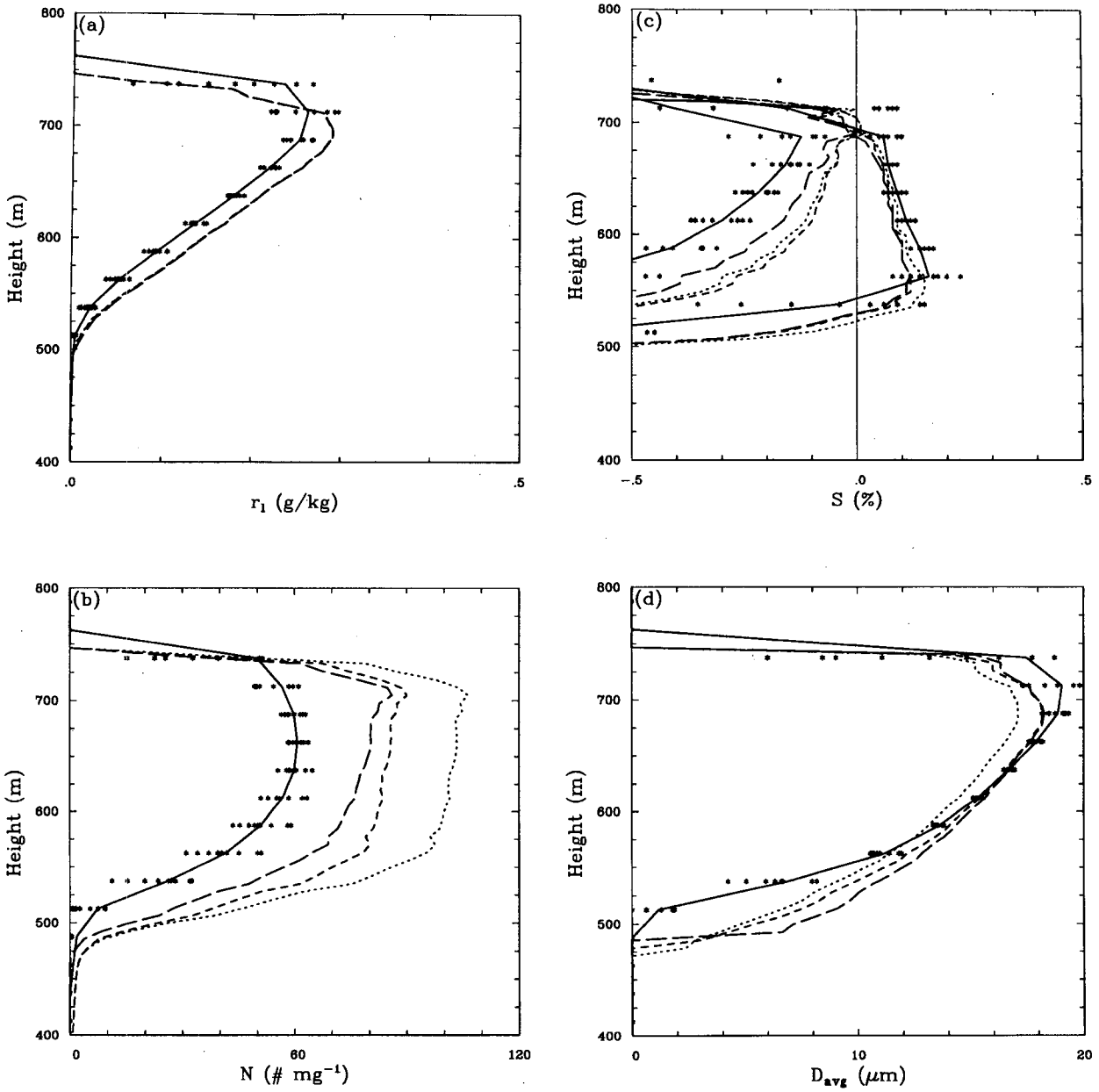

FIG. 10. Comparison of mean microphysical profiles: (a) liquid-water mixing ratio; (b) number mixing ratio (units approximately the same as number per cm^3); (c) supersaturation (only updraft and downdraft averages plotted); (d) mean diameters (plotting threshold of 5 drops per cm^3 used). Experiment LES-BM (solid line), experiment TEM-ENK (long dash), experiment TEM-LNK (short dash), experiment TEM-LWK (dotted line). Scattered points at each level represent layer means from LES-BM at different times.

the lack of inclusion of layer-wise entrainment in the TEM data.

The mean number of activated drops is significantly larger in TEM-ENK than in the LES-BM experiment (Fig. 10b). This is the consequence of two different processes. The most dominant process is explained through a consideration of downdraft averages. In the LES-BM data, downdrafts have considerably fewer drops (of order 20%) than updrafts (see Fig. 7b), in contrast to the TEM data in which downdrafts actually have marginally more drops than downdrafts in association with higher cloud-top supersaturations and secondary activation at cloud top. For the reasons discussed in Stevens et al. (1996), the reduction in the number concentration in the downdrafts in the LES-BM may be largely an artifact of the inability of the model to track a cloud boundary through a grid box. Because the reduction in drop number in downdrafts

occurs at cloud top, and because the TEM uses the identical numerical routines in this comparison, it is clear that the differences do not arise from such factors as enhanced dispersion in the evaporation calculations. The second and less dominant process is attributable to the activation of fewer drops in LES-BM updrafts attributable to a slight under-representation of the cloud-base supersaturation caused by the spatial averaging in the Eulerian dynamical model. The effect of spatial averaging on cloud-base supersaturations is illustrated by Clark (1974b) using a simple column model and prescribed updrafts, and is confirmed here in a much more general setting. In our simulations this problem leads to an underestimation of about 10% in the number of drops activated at cloud-base in the LES-BM data relative to what is predicted using the TEM with identical microphysics. More generally, the magnitude of the error will depend on the aerosol activation spectrum.

Although the LES-BM activated fewer drops in the updrafts, the updraft supersaturations are higher at cloud base (Fig. 10c). This is due to the fact that the locations of the cloud-base updraft maxima in the LES-BM are better spatially correlated with one another and exhibited a smaller variance. Supersaturations in the TEM occasionally rise to as high as 1%, which is more than twice as high as the largest values of cloud-base supersaturation predicted by the LES-BM. They are also more spatially peaked across a greater range of levels so that the magnitude of the layer averaged maxima is filtered out in the averaging procedure. This indicates that updraft-averaged supersaturations are only a weak indicator of drop number activation. Differences among the models in their respective estimates of mean diameter (Fig. 10d) can be accounted for by differences in the number of activated drops.

As for the case of the mean fields there is strong agreement in the qualitative structure of the dispersion fields among the models. In particular, the liquid water dispersion (Fig. 11a) compares well quantitatively and qualitatively, which is evidence of the strong thermodynamic controls on this field. In the number concentration data (Fig. 11b) there is a slight quantitative disagreement in the midcloud dispersion minima, which is directly proportional to variations in the mean value. The dispersion of the relative humidity (Fig. 11c) shows a peak only near cloud top where there is the greatest contrast in the moisture content of the air. The nearly zero dispersion within the cloud is a reflection of the fact that phase changes act to minimize the variance in relative humidity at the expense of the sensible temperature. Similarly, the dispersion in the relative humidity field (Fig. 11c) is quantitatively similar among the models, although the in-cloud minimum is larger for the simulations with smaller drop concentrations and larger supersaturation phase relaxation times.

Quantitative agreement is poor in comparisons of the diameter dispersion (Fig. 11d). Though differences in cloud-top and cloud-base values are sensitive to the sampling criteria, the relatively smaller value of drop size dispersion in the heart of the cloud as represented by the LES-BM is robust. This appears to be the result of the subfilter mixing in the vertical occurring between drop parcels in the LES-BM data. Filter-scale mixing is modeled as diffusion in the Eulerian domain and can be thought of as an averaging on the filter scale. This is in marked contrast to the TEM data, which is not averaged, nor mixed, before the compilation of statistics. In addition, because the average mass may vary in a drop bin, the two-moment Eulerian representation of drops does not conserve the variance in the droplet spectrum upon mixing, but acts marginally to reduce it.

2) EFFECT OF EULERIAN MASS SPACE REPRESENTATION

Here the LES-BM data will be abandoned in favor of comparisons among the data generated by the TEM with differing microphysical frameworks. First, experiments TEM-ENK and TEM-LNK are compared in order to test assumptions about the activation parameterization, and the effect of averaging in mass space implicit in the Eulerian microphysical formulation. The Lagrangian growth routines used in experiment TEM-LNK neglected gas kinetic effects in order to be more consistent with the growth routines represented by the Eulerian microphysical package.

Although much of the data agrees quite well, there are two important differences, the first of which is associated with the treatment of the drops in their earliest stages of growth. Because the Eulerian microphysical scheme must activate drops near the size of the lowest bin, the earliest stages of growth are overpredicted in experiment TEM-ENK. This allows activation to absorb the generation of excess vapor in updrafts more rapidly, so that cloud-base supersaturations do not grow quite as high, and the number of activated CCN is reduced (see Figs. 10b and 10c). The quantitative impact of this error will depend largely on the structure of the aerosol distribution. In our simulations it represents about a 10% decrease in the number of activated drops, which is associated with about a 0.25-μm change in the average diameter.

The second major difference is revealed by a comparison of the values of the drop size dispersion in Fig. 11d. The Eulerian microphysical model yields larger values of dispersion through the depth of the cloud. The primary contribution to the large values of layer averaged dispersion is from the downdrafts. Off-line tests show that the Eulerian condensational routines generate spuriously large amounts of diffusion during the evaporation process. This is not a problem in the updrafts where, because of the log spacing of the drop-binning intervals, condensational growth forces the drop spectra into ever broader size bins. Dispersion in the downdrafts leads to the simultaneous generation of

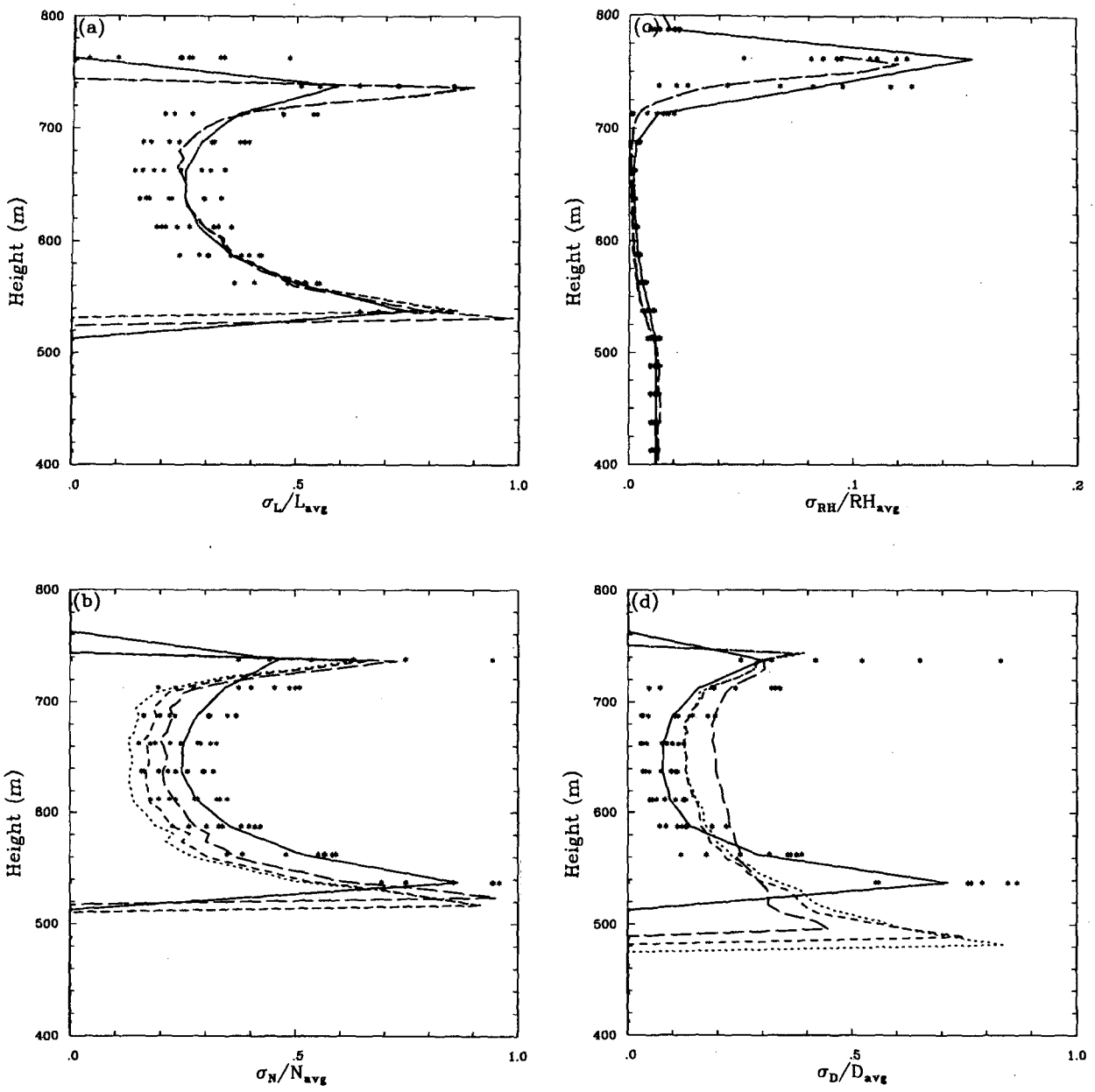

FIG. 11. Comparison of dispersion profiles of (a) liquid-water mixing ratio; (b) number mixing ratio (units approximately the same as number cm^{-3}); (c) relative humidity; (d) mean diameters, plotting threshold as in previous figure. Lines chosen as in previous figure.

too many small and large drops at the expense of median-size drops. This leads to premature evaporation of the small drops, and postponed evaporation of the larger drops, smearing out cloud base in the downdrafts. The slightly larger increase in height evident in the number concentration profile generated with the Eulerian microphysics (cf. slopes of long- and short-dashed lines in Fig. 10b), is a consequence of this problem. Liu et al. (1995) show how the use of variational methods to solve the evaporation equation in one-moment schemes or the Egan and Mahoney approach in multiple-moment schemes will significantly reduce the dispersion; although they did not compare these approaches with the semianalytic method of Tzivion et al. (1989) used here; this matter is pursued in the discussion.

3) GAS KINETIC EFFECTS

The impact of neglecting gas kinetic effects is compared within the framework of the TEM with Lagrangian microphysics. The simulation with gas

kinetic effects (experiment TEM-LWK) is represented by the dotted lines in Figs. 10 and 11. Compared to the identical simulation without gas kinetic effects (short dashed line), we note that there are substantial differences in the values of the maximum cloud-base supersaturation. As a consequence, there are large differences in the number of CCN that activate into cloud drops. The basic reason for this is that gas kinetic effects retard the growth of the smallest drops, thereby increasing the phase relaxation time of the supersaturation field, which leads to the development of larger cloud-base supersaturations. In presenting a similar result in the context of simple numerical experiments, Clark (1974b) credits Rooth (1957) with first explaining this process some 20 years earlier. Notwithstanding that this process has been well understood for nearly 40 years, the magnitude of the quantitative difference is surprising.

b. *Microphysical structure of contributing trajectories*

To understand how different physical processes contribute to the simulated cloud microstructure, four sensitivity tests are conducted. All simulations are conducted with the TEM coupled to the Lagrangian microphysical component with gas kinetic effects included. These four sensitivity runs and the control run are plotted in Figs. 12 and 13. In the first sensitivity run (experiment S1) mixing is turned off so the conserved variables are held constant at their initial values. The second sensitivity run (experiment S2) differs from the first in that the adiabatic values of θ_l and q_T no longer differ among the trajectories, but are instead specified to take on the average initial value of the associated variable in the full dataset. The third sensitivity run (experiment S3) differs from the second in that the vertical velocity is now kept fixed along the trajectory. The fourth and last sensitivity run (experiment S4) differs from the third in that data is only collected along an updraft segment of one of the trajectories, thereby providing a measure of the background statistics. The sensitivity runs are tabulated for easier reference in Table 2, and represent increasing degrees of uniformity in the trajectory set.

TABLE 2. Features of sensitivity simulations conducted with the TEM. "Homogenized" in headings refers to the prescription of a uniform initial condition or vertical velocity. Initial conditions, when homogenized, are done at the mean value. Vertical velocities are homogenized with magnitude 0.5 m s^{-1}.

Experiment name	Adiabatic trajectories?	Homogenized initial conditions?	Homogenized w?	Number of contributing trajectories
Control	no	no	no	full set
S1	yes	no	no	full set
S2	yes	yes	no	full set
S3	yes	yes	yes	full set
S4	yes	yes	yes	single updraft

1) MEAN FIELDS

In experiment S1 the absence of mixing increases the liquid-water content of the cloud relative to the control (Fig. 12a). This is particularly evident in the downdrafts (conditionally averaged profiles not shown). Because the liquid-water content is greater, but number concentrations are relatively unchanged (Fig. 12b), there is an approximately 1.5-μm increase in the average diameter of drops at every height (Fig. 12d). Another interesting aspect of mixing (not revealed by the figures) is that in the absence of mixing across cloud top, the net transport of liquid water is out of cloud base as nonzero phase relaxation times in the supersaturation field make downdrafts slightly moister than updrafts at a given level. This is in marked contrast to the control run, where downdrafts are significantly drier than updrafts, due to entrainment across cloud top, and the net flux of liquid water is into the cloud.

In S1 there are large increases in the cloud-base values of supersaturation (Fig. 12c), in both up- and downdrafts, but despite a slight lowering in cloud base there is effectively no change in the number concentration (Fig. 12b). This is yet another illustration of how mean supersaturations, even conditionally averaged over updrafts, are not a reliable indicator of cloud-drop concentration. These points are even further emphasized by a consideration of the remaining experiments, where increasing uniformity in the ensemble of trajectories leads to flatter but quantitatively unchanged number concentrations, better defined cloud base, and stronger mean cloud-base supersaturations, derived from more coherency in the trajectories. Because a vertical velocity of 0.5 m s^{-1} (experiments S3 and S4) generates approximately the same number concentrations as the full ensemble of trajectories, this velocity may be considered an equivalent vertical velocity responsible for activating the average number of particles. It roughly corresponds to the square root of the variance in w, and generates a supersaturation of 0.6%. Notwithstanding that such a supersaturation is larger than that produced in the LES-BM simulations, it is still well within the observational constraints.

2) DISPERSION FIELDS

In experiment S4 the background dispersion near cloud base is shown to be significant (Fig. 13), with standard deviations on the order of the mean. The order of vertical variability on 7-m sampling intervals also leads to marginal values in the background dispersion above cloud base, for both the liquid water and diameter fields. Increasing homogeneity in the trajectory set tends to decrease the depth of the cloud-base maxima

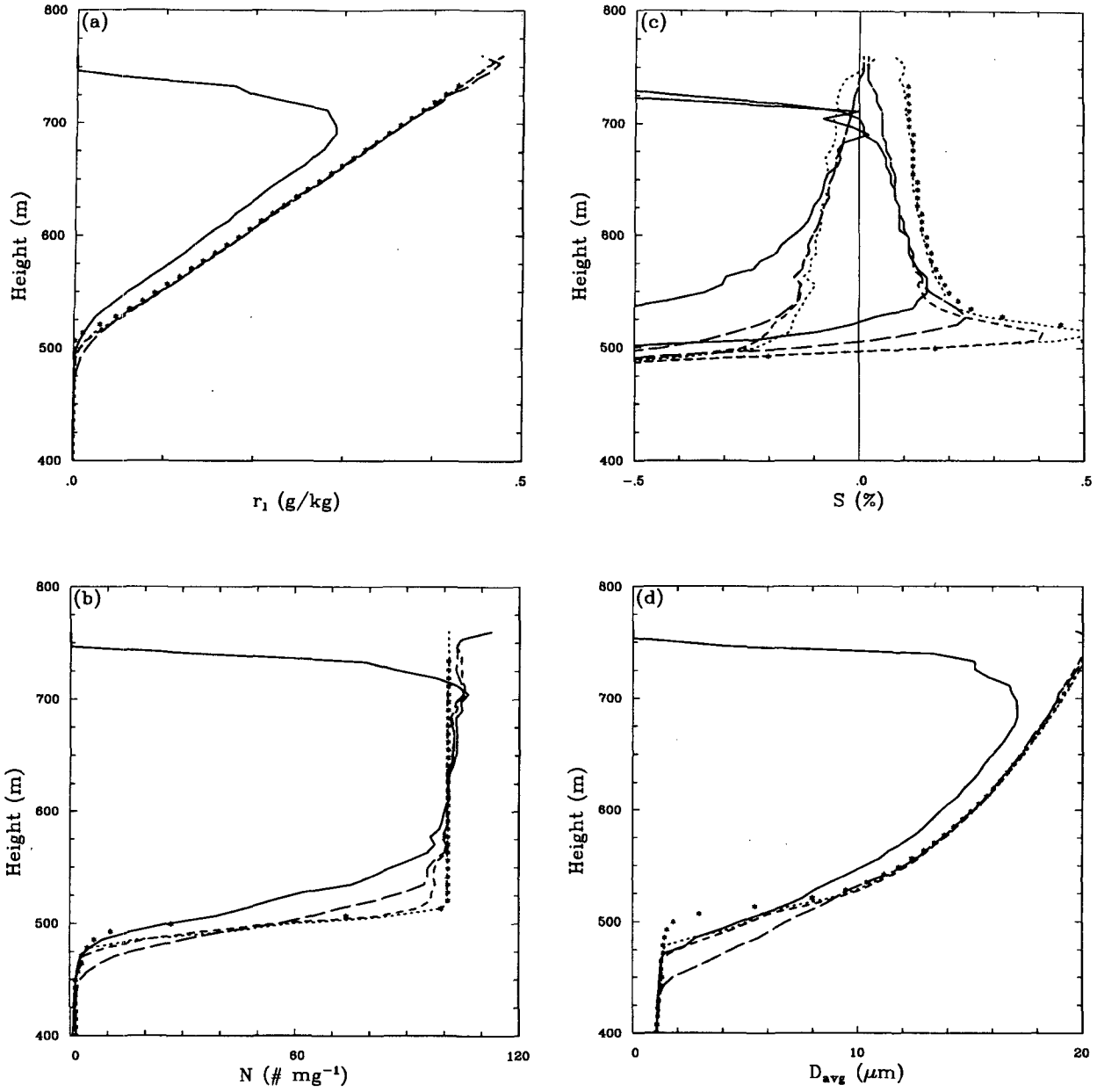

FIG. 12. Mean microphysical fields as in Fig. 11 but for five different experiments. Control (solid line); experiment S1 (long dash); experiment S2 (short dash); experiment S3 (dotted line); experiment S4 (scattered points).

in dispersion, largely as the variability in the cloud-base height is diminished. The control run is the only one with strong cloud-top dispersion in all fields since it is the only simulation in which mixing across cloud top is represented.

Comparing the control with experiments S2 and S1 illustrates that half the dispersion in the liquid water (Fig. 13a) is a consequence of subcloud variability (previous mixing) and half is the product of mixing that occurs over the course of the evolution of the trajectory ensemble. Since the simulation is initialized to be horizontally homogeneous, all subcloud variability reflects the history of previous mixing. Different boundary layers may be able to support different amounts of variability in thermodynamic fields, and consequently, differing amounts of dispersion in the cloud microphysical structure.

Experiments S1 and S2, respectively, have about 55% and 45% of the diameter dispersion of the control (see Table 3 and Fig. 13d). So although subcloud variability in lifting condensation levels (the difference between S1 and S2) is an important contributor to the

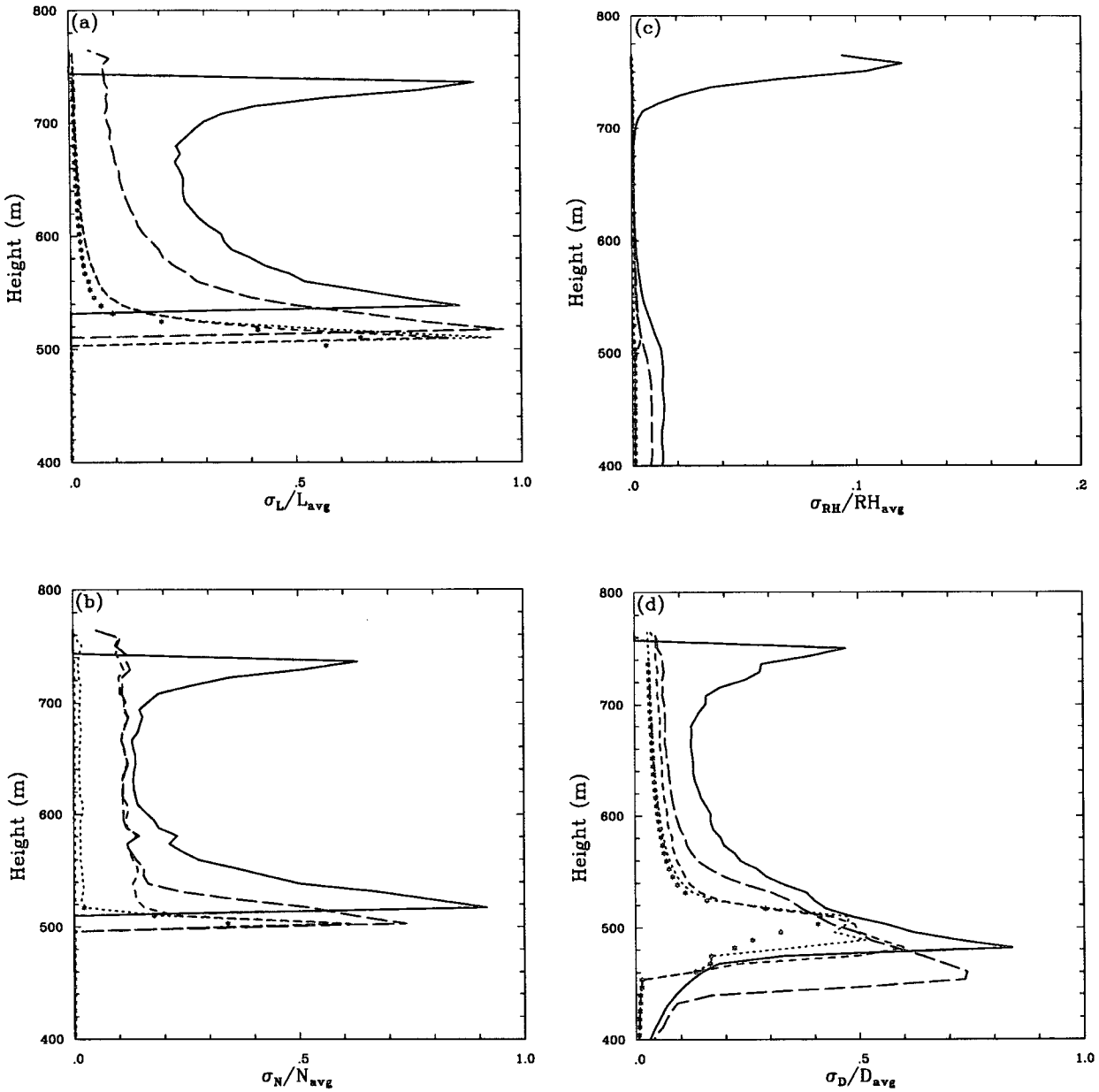

FIG. 13. As in Fig. 12 but with line designation as in previous figure.

diameter dispersion, it is not as large a source for simulated diameter dispersion as is mixing across cloud top. Moreover, most of the mixing across cloud top generates dispersion in the downdrafts, while subcloud variability leads to approximately equal amounts of dispersion in the up- and downdrafts. Correlations between the dispersion in the subcloud CCN concentrations and updraft velocities (for instance consider increasing CCN concentrations closer to the surface and stronger updrafts associated with more surface layer air) can provide an additional source of dispersion not represented by these simulations. In contrast, the liquid water dispersion in S1 is about half that of the control, while nearly all the dispersion is eliminated in S2, so subcloud variability and cloud-top entrainment contribute approximately equally to the dispersion in this simulated field.

Experiment S3 is designed to minimize the variance in activating velocities, while maintaining the impact of differing parcel histories on microphysical variability. In contrast S4 looked at characteristic values of dispersion in an isolated updraft. We found that ho-

TABLE 3. Values of dispersion for different fields from different simulations at 650 m.

Experiment	$\sigma_{qL}/\overline{qL}$	$\sigma_N/\bar{N}$	$\sigma_D/\bar{D}$
Control	0.252	0.138	0.129
S1	0.110	0.116	0.071
S2	0.017	0.116	0.059
S3	0.019	0.014	0.042
S4	0.014	0.000	0.040

mogenizing the vertical velocities virtually eliminated the dispersion in the number concentration field, and further reduced the diameter dispersion to 33% of the control, near its baseline value of 31% predicted by experiment S4. Because much of the variability associated with different time-history vectors of trajectories within a cloud (given the same activated cloud-drop spectrum) is due to variations of vertical velocity not just at cloud base but also within the cloud, this particular experiment does not fully represent the variability due to differing parcel histories—at best it bounds it from below.

The inability of the well-represented processes, such as the turbulent generation of varied trajectories that leads to varied updraft histories, to generate the required values of droplet diameter dispersion suggests that the remainder of the observed dispersion must be generated by other means. The representation of cloud-base turbulent motions on finer scales may increase the dispersion due to a greater variety of activated distributions; however, given the range of updraft velocities represented by the trajectory set significant increases are not anticipated. Other possible processes include in-cloud mixing among parcels and mixing across cloud interfacial boundaries. The former process (which depends on the fact that drops are not parcel-wise conservative) is not represented, and the latter is poorly represented in all of our simulations, so it is difficult to comment on the quantitative partitioning of dispersion between the two processes.

6. Discussion

a. *Cloud-top supersaturations*

Sharp gradients in thermodynamic properties at cloud top pose difficult problems for the numerical operators in Eulerian models. In particular, an accurate prediction of the supersaturation field at cloud top has eluded most cloud models (e.g., Grabowski 1989; Kogan et al. 1994; Feingold et al. 1994). In an illuminating study, Grabowski and Smolarkiewicz (1990) illustrate how this problem may be mitigated by an improvement in one's numerical operators and choice of thermodynamic variables. Stevens et al. (1996) argued that in addition to the truncation error contributions to cloud-edge supersaturations, the ubiquitous assumption whereby microphysical processes are driven by grid-averaged thermodynamic quantities leads to significant and spurious supersaturations as a cloud advects through a gridbox.

Stevens et al. (1996) show how the production of cloud-top supersaturations in the Eulerian dynamical framework result from the assumption that grid-averaged thermodynamic quantities can be used to force the microphysical processes. However, such an assumption is not explicit in the TEM framework, yet it too suffers cloud-top supersaturation peaks. To understand this phenomenon, the trajectories that experienced secondary cloud-top peaks in the supersaturation (greater than 0.5%) are examined; all of them evolve through a cycle of warming and drying followed by cooling and moistening immediately prior to the supersaturation maximum, as illustrated by Fig. 14.

To demonstrate the spurious nature of mixing along trajectories that cross cloud interfacial boundaries, it is necessary to consider a trajectory crossing from a grid volume that is saturated to one that is subsaturated. In the LES-BM, the advected parcel (from which the trajectory data is driven) will warm and dry on the timescale of this crossing (i.e., in a time step) and not on some natural mixing timescale determined by local parcel-scale properties of the flow. In such situations the mixing timescales are much longer than the advective timescales, and our representation of trajectory evolution will be erroneous. In some sense, the excursion of trajectories above cloud top may represent the motion of cloud top into the next higher grid volume, where

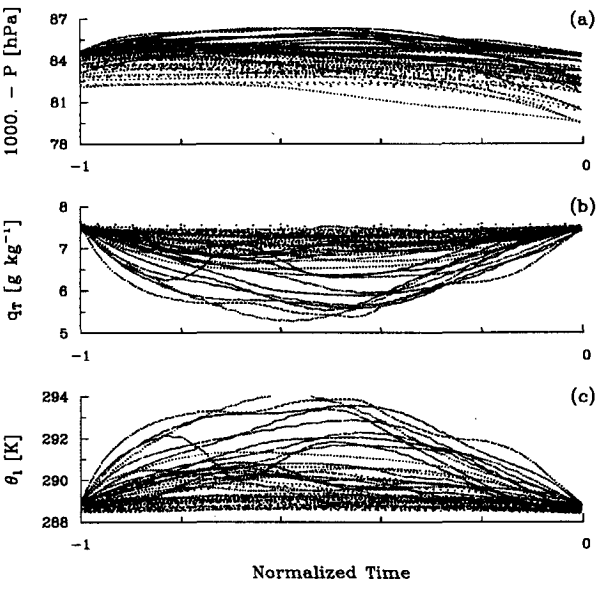

FIG. 14. Scatterplot of (a) pressure, (b) total-water mixing ratio, and (c) liquid-water potential temperature along cloud-top trajectories that lead to secondary maxima in supersaturations at time = 0. The time dependence of the trajectories is normalized by the total amount of time they spend in a subsaturated environment.

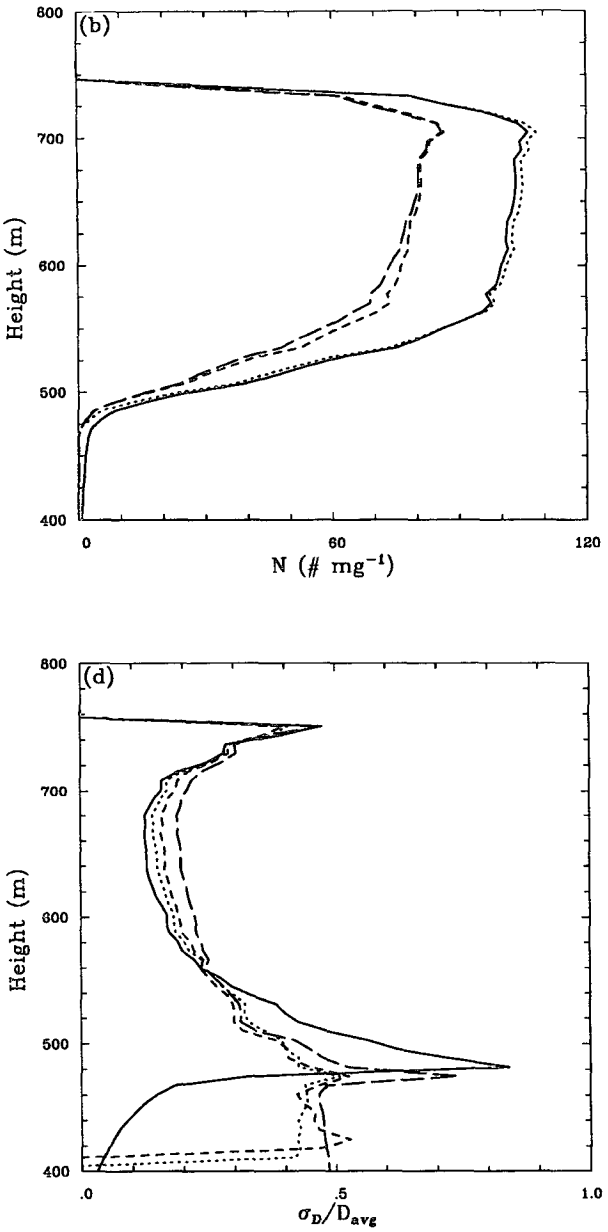

FIG. 15. Comparison of profiles of (a) number concentrations, and (b) diameter dispersion. Experiment TEM-LWK (solid line), experiment TEM-ENK (long dash), experiment TEM-ENK with new condensation routine, and no gas-kinetic effects included (short dash) experiment TEM-ENK with new condensation and gas kinetic effects (dotted line).

such motion is not significant enough to saturate the next grid volume and hence is not represented by the model. The parcels are thus too rapidly dried and warmed along the trajectories as illustrated in Fig. 14, thereby generating anomalous cloud-top supersaturations upon their simulated reentry into the cloud layer. To mitigate this problem, one can model mixing using a more detailed method, which makes use of the difference between the parcel's state and that of the environment as well as the local deformation. Unfortunately, such an approach still requires a specification of an entrainment rate for which our model gives little guidance. Nevertheless this approach is an area of active research.

b. Calculations of condensation and evaporation

As this study reveals certain deficiencies in the condensation–evaporation calculations (i.e., the Tzivion et al. 1989 method is too dispersive and did not account for gas kinetic effects) alternative approaches are considered. Significantly better solutions (both faster and more accurate) are obtained by using a new remapping scheme and a simple parameterization of gas kinetic effects. Details of this new method are given in the appendix, while results are plotted in Fig. 15a. This figure shows the resultant number concentration profiles produced by the new scheme, compared to the experiments TEM-LWK and TEM-ENK. Results both with and without gas kinetic effects are plotted. The inclusion of the gas kinetic effects is very well represented by the new method (in generating these data we chose $l_0 = 4$ μm (see appendix)); moreover, the number concentrations are also somewhat flatter and the more limited values of dispersion in the new approach reduced by half the discrepancy in values of diameter dispersion evident in comparisons of TEM-ENK and TEM-LWK (see Fig. 15b).

c. Trajectory timescales

Given that a number of important processes (e.g., oxidation rates in aqueous phase chemistry and precipitation formation) are strongly dependent on in-cloud

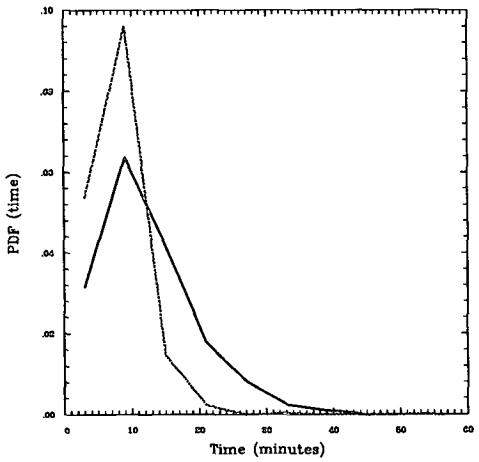

FIG. 16. The probability density function showing the distribution of times spent by different trajectories in cloud. (3D simulation given by solid line, 2D simulation given by dashed line).

residence times, the trajectory dataset has been analyzed in order to develop a better estimate of the distribution of such timescales as simulated by the LES. Results of this analysis are plotted in Fig. 16. Although the dominant timescale is on the order of a large eddy turnover time (≈12 min) the distribution of timescales is relatively broad. Consequently a certain favored subset of trajectories (e.g., the trajectory in the top panel of Fig. 9) recirculate within the cloud, thereby prolonging their in-cloud residence time. For the sake of comparison we also ran the Eulerian cloud model in two dimensions. The trajectory structure produced in the two-dimensional simulation of the same case has a considerably narrower spectrum of timescales. The lack of a significant long timescale tail results in a significantly smaller mean timescale of 8 min (notwithstanding that in both the two- and three-dimensional simulations the most common timescale is on the order of 8 min). This points to one limitation of two-dimensional simulations. Others will be addressed in a separate study.

Our calculations of condensational growth neglect radiative effects. However, a number of investigators (e.g., Barkstrom 1978; Austin et al. 1995; Ackerman et al. 1995) have indicated that radiative effects may be important in the evolution of cloud-top cloud-drop spectra, particularly if cloud-top residence times are long. With this in mind, the cloud-top residence times of the trajectory set are also investigated. Figure 17 illustrates the frequency distribution of the time over which trajectories are continuously suspended above 700 m. Summing over all classes indicates that approximately 35% of the trajectories exceeded the 700-m level during at least one point in their evolution. Most of the trajectories that reach 700 m spend less than 7.5 min at cloud top, with the most frequent class spending between 2.5 and 5 min near cloud top. However, a significant fraction of the trajectories (about 8% of 500) spent more than 10 min at cloud top. Assuming the cloud-top portion of our trajectory ensemble represents the realistic evolution of a parcel, it appears that radiative effects may be important to the dynamical evolution of the cloud-drop spectra—although the neglect of subgrid energy in the velocities used to advect parcels probably leads to an overestimate of cloud-top residence times in the above analysis.

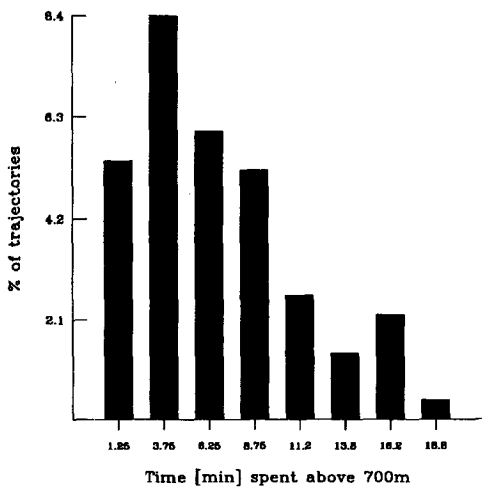

FIG. 17. A histogram showing the frequency of different time intervals, where the time intervals correspond to the amount of time a parcel spends above 700 m.

d. Relationship to other work

In a relevant analytic attempt at treating some of the ideas addressed in this study, Cooper (1989) developed a theoretical framework for understanding droplet spectral broadening associated with the condensational growth of drops along turbulent trajectories. Although it would be of interest to examine our results in light of his work, fundamental differences between the approaches make the value of such a comparison dubious. The differences in approach are in themselves interesting, however, as they better illuminate the nature of the present work.

Cooper (1989) examined the contribution to spectral broadening in parcels of air on the order of meters and argued that to leading order the dominant contribution (within the regime of validity of the equilibrium supersaturation approximation) is due to two terms: (i) the fluctuations in the integral radius along the trajectories of individual drops, which end up constituting the drop spectrum at a given time and place; (ii) the correlations in fluctuations of integral radius and vertical velocity along the same trajectories. In all cases fluctuations are evaluated with respect to the ensemble average of the integral radius and vertical velocity over all constituent trajectories. Instead of looking at broadening on the parcel scale, the present work looks at the contribution to broadening at a fixed level and on space and timescales of $O(1000\ \text{m})$ and $O(1000\ \text{s})$, respectively. Moreover, and perhaps more significantly, the present work does not consider the trajectories of individual drops, but rather of individual parcels of air with which an initial aerosol population (and subsequent drop distribution) are assumed to remain coincident. In other words, and in contrast to Coopers work, a four-dimensional space-time rendering of the trajectories studied herein do not cross. These fundamental differences, make it impossible to formally evaluate the different terms in his formulation.

Nevertheless there is one element of Cooper's (1989) analysis that we may begin to address within the current framework. That is the contribution to spectral broadening from differential cloud-base activation. By equating the differential of the ln of a function with its dispersion [i.e., by setting $d(\ln x) = \sigma_x/\bar{x}$] and on the basis of a simple representation of cloud-drop activation (which assumes that aerosol activation is pro-

portional to supersaturation raised to the power K), Cooper obtained the following relationships between updraft (w), number concentration (N) and diameter (D) dispersions:

$$\frac{\sigma_D}{\bar{D}} \approx \frac{1}{3}\frac{\sigma_N}{\bar{N}} \approx \frac{K\sigma_w}{(4+2K)w}. \quad (15)$$

Comparing $\sigma_N/\bar{N}$ to $\sigma_D/\bar{D}$ in Fig. 13 shows that $\sigma_D/\bar{D}$ is approximately equal to $\sigma_N/\bar{N}$ for simulated mixing (control experiment). For adiabatic parcels it is also about equal to $\sigma_N/\bar{N}$ near cloud base, but falls off to about $\frac{1}{2}\sigma_N/\bar{N}$ toward cloud top. Noonkester's (1984) observations of nonprecipitating stratocumulus concur with the simulations in that diameter and number dispersion are about equal. Only for the relatively small dispersion profiles generated assuming constant updraft velocities (experiment S3) is Cooper's one-third relation between number concentration and diameter dispersion characteristic of the data. This suggests that distributions are sufficiently large to render the assumption that $d(\ln x) = \sigma_x/\bar{x}$ a poor one.

The trajectory updraft data gives $\sigma_w \approx 0.24$ and $\bar{w} \approx 0.56$ m s^{-1}. Subtracting the dispersion in experiment S3 from that in experiment S1 yields an estimate of $\sigma_D/\bar{D}$ due solely to differential cloud-base activation: $\sigma_N/\bar{N} \approx 0.04$. So that in order to evaluate Eq. (15) all that is needed is an estimate of K. Unfortunately, in contrast to Coopers (1989) analysis (which is based on Twomey's activation scheme, which assumes a Junge distribution), our data is derived on the assumption that the lognormal-distribution function better characterizes the aerosol. This means that the activation spectrum is characterized by a range of K depending on the supersaturation, thus making a direct comparison between our data and Cooper's relation (which for reasonable ranges of K is approximately linear in K) difficult. Notwithstanding that reasonable values of K may be chosen so as to allow Eq. (15) to capture the simulated values of diameter dispersion, agreement is probably fortuitous; especially when it is recalled that a key step in the derivation (i.e., the relation between diameter and number concentration dispersion) is not well represented by the data.

e. *Relationship to observations*

Because the TEM took for granted the dynamical framework provided by the LES, comparisons between models—while instructive—are also limited. In particular, we are only able to assess to what extent the LES-BM derived microphysical solutions are consistent with the simulated trajectory structure of the cloud. Clearly there is room for further evaluation. While a qualitative comparison of the model to observations of stratocumulus by Noonkester (1984) and Nicholls (1984) did indicate rough agreement in normalized statistics, it is still not clear whether the right answers are predicted for the right reason. Models of the class of the LES-BM are much more limited by resolution then they are by their physics, and while a classic test of a model so limited is one of convergence at increasing resolution, computational limitations render such an approach impracticable.

There does exist, however, the observational capability to more accurately constrain the model. The relevant pieces of the condensation-nucleation puzzle are the probability density function of w, which can be measured in nondrizzling clouds using a K_α-band radar (Frisch et al. 1995), and below cloud using lidar; CCN spectra in the range of supersaturations below 1.5% (e.g., Hudson and Frisbie 1991); the vertical thermodynamic structure of the boundary layer, measurements of the in-cloud droplet spectrum and the cloud-top radiative forcing (all of which can be generated using an adequately configured tethered balloon). A more constraining test for the model would be to then see if it can simulate all the pieces of this puzzle to within the experimental accuracy of the measurements. While all these measurements can in principle be made (as indicated), they have to our knowledge not been made simultaneously.

The LES-BM is clearly unable to represent features that exist at scales below the resolved scales, which with current computational capabilities are on the order of scores of meters. It is, however, unclear to what extent inhomogeneity on scales smaller than this are important in regulating the macroscopic microphysical behavior of the cloud (i.e., quantities like drizzle). Laboratory experiments in mixing layers at moderate Reynolds numbers have indicated that inhomogeneities introduced at the scale of the largest eddies may be quite long lived (Breidenthal 1981). For instance, the model proposed by Broadwell and Breidenthal (1982) estimates that large-scale inhomogeneities may persist for up to an eddy turnover time (about 10 min) until they are stretched and folded to a scale where diffusive effects are important. While clouds differ from mixing layers in several important respects[2] the suggestion that considerable structure exists below the resolved scales of the model requires more detailed observations focused on particular questions that relate this structure to large-scale features. For instance, using models such as the LES-BM to make falsifiable hypotheses about the relationship between entrainment, drizzle, and fine-scale structure (or lack thereof) in the cloud would appear to be a fruitful avenue of investigation.

7. Summary

A dynamical model coupled to a detailed representation of the droplet spectrum (the LES-BM) has been

[2] They are two-phase flows, have considerably larger Reynolds numbers, and the coherent structures are more plume like.

developed for the study of a variety of processes in the stratocumulus-topped marine boundary layer. Simulations of the condensation–nucleation problem for an idealized stratocumulus layer are evaluated on the basis of observations and results from simple parcel models integrated over an ensemble of trajectories produced by the LES. The comparisons reveal that although the LES-BM is able to realistically simulate many microphysical features of observed stratocumulus, relatively fine vertical resolution, and some representation of gas kinetic effects are important in representing cloud-base activation properly. A new condensation–evaporation scheme is derived to include gas kinetic effects and reduce the amount of numerical dispersion associated with the original calculations. Perhaps the most vexing problem for the LES-BM is its inability to resolve the mixing process across cloud interfacial boundaries. Within a gridbox all mixing is taken to be homogeneous and microphysical calculations are driven by grid-averaged thermodynamic quantities. Both approaches probably lead to significant errors. Lastly, due to the nonlinear dependence of processes like precipitation formation and radiation on the characteristics of the droplet distribution, it is not clear to what extent small errors in the representation of the latter will lead to more significant errors in the former.

The simulations illustrate how the microphysical structure of the cloud is a strong function of the turbulent circulations and that models that fail to resolve these circulations will, in the absence of its adequate parameterization, be unable to reproduce many aspects of cloud microphysical structure. Although two-dimensional simulations appear to well resolve the basic features of boundary-layer eddies (e.g., Feingold et al. 1994), it is shown that their timescales differ considerably from their three-dimensional counterparts.

On the basis of the trajectory analysis it is shown that values of diameter dispersion predicted in the absence of mixing, while significant, are a factor of two-to-five smaller than commonly observed values of order 0.2. Consequently, mixing and perhaps other mechanisms are likely to be important; notwithstanding that mixing as represented in the Eulerian cloud model led to reduced values of dispersion. Observed values of dispersion in the number concentration are explainable solely on the basis of trajectories having different updraft velocities. Moreover, they are on the same order as values of diameter dispersion leading to disagreements of about 100% when compared to Coopers (1989) result that suggests that the latter should scale as one-third of the former.

Trajectory timescales are evaluated and it is found that the simulated trajectories spend on average 7 min in cloud. Cloud-top residence times, while perhaps overestimated, are often on the order of 10 min or longer, thus suggesting that radiational processes may have sufficient time to significantly impact the nature of the cloud drop spectra.

Acknowledgments. We thank Chin-Hoh Moeng for her helpful comments with regard to this manuscript; Wojciech Grabowski for fruitful conversations regarding the production of cloud-top supersaturations; Piotr Smolarkiewicz and Craig Tremback for their help with the flux-corrected transport methodology; as well as Phil Austin, Yefim Kogan, and an anonymous reviewer for their numerous suggestions all of which greatly improved this paper. Bjorn Stevens is grateful for his funding from a NASA/EOS Global Change Fellowship. We also would like to acknowledge funding from the U.S. Department of Energy under Contract DE-FG03-9YER61749 and through the National Institute for Global Environmental Change, Research Agreement Number NIGEC-91-S01.

APPENDIX

New Condensation/Evaporation Calculations

The basic approach of the Tzivion scheme is common to all semi-Lagrangian schemes in which drops are grown according to a Lagrangian representation and a simulated distribution function is remapped back to an Eulerian grid. In some semi-Lagrangian schemes, the drops are grown on small time steps and the supersaturation field evolves freely over the small time steps (e.g., Kogan 1991). The Tzivion scheme, however, is designed to grow drops over longer time steps according to the analytic solutions to their growth rates consistent with the time integral of the supersaturation field provided by the semianalytic solutions to the supersaturation equation. This scheme takes advantage of the fact that a growth equation of the form:

$$\frac{dm}{dt} = \phi(m)k(t), \tag{A1}$$

generally allows analytic solutions. Tzivion et al. (1989) assume $\phi(m) = m^{1/3}$ for which the analytic solution is the well-known form

$$m(t + \delta t) = \left(m_0^{2/3} + \frac{2}{3}\tau\right)^{3/2},$$

where

$$\tau \equiv \int_t^{t+\delta t} k(t')dt', \tag{A2}$$

and $m_0 \equiv m(t)$. Moreover, by linearizing the zeroth and first moments in a bin, a distribution function can be constructed that also yields analytic solutions for the remapping. Unfortunately, including gas kinetic effects generally requires the inclusion of a mass dependence in the thermodynamic term $C(p, T)$, which precludes the possibility of analytic solutions. However, it has been shown (Clark 1974a) that gas kinetic effects may be well represented by assuming that $\phi(m) = m^{2/3}/(m^{1/3}$

$+ l^*$), where l^* corresponds to a length scale: $l^* = l_0(\frac{4}{3}\pi\rho_l)^{1/3}$, with l_0 of order 5 μm. In this case analytic solutions to Eq. (16) may still be found, namely:

$$m(t + \delta t) = \left[\left((m_0^{1/3} + l^*)^2 + \frac{2}{3}\tau\right)^{1/2} - l^*\right]^3 \quad \text{(A3)}$$

and analytic solutions to the remapping can also be solved for.[3]

However, the analytic solutions to the remapping based on the assumption of linearized moments are far too cumbersome to be numerically attractive. For this reason, a remapping scheme based on assumed top-hat distributions is derived, where the impetus for such a remapping came from the moment conserving techniques of Egan and Mahoney (1972). In contrast to Egan and Mahoney, where the second moment is prognosticated in order to predict the width of the top hat, we diagnose a measure of the width of a top hat, R_j, in the jth bin based on two heuristic methods. The first method is to choose the largest width consistent with the mean mass and the assumption that all the mass must be contained within a bin:

$$\frac{R_j}{2} = \min\left(x_{j+1} - \frac{M_j}{N_j}, \frac{M_j}{N_j} - x_j\right). \quad \text{(A4)}$$

The second method used the relation between the variance σ^2 and width of a square pulse distribution such that $R_j = (12\sigma_j)^{1/2}/\Delta x_j$, where Δx_j is the width of the jth bin and σ_j is the standard deviation of the distribution within it. Because we do not solve for the second moment within a bin, we must use the closure assumption of Tzivion et al. (1987) to relate the second moment in the jth bin, Z_j, to the zeroth, N_j, and first moments, M_j, so that $Z_j = (\xi_j M_j^2)/N_j$ with closure parameter $\xi_j \equiv \frac{1}{2} + \frac{3}{2}(N_j x_j/M_j) - (N_j x_j/M_j)^2$, where x_j is the lower mass limit of the jth bin. Given these definitions, the value of σ_j follows:

$$\sigma_j^2 = \frac{Z_j}{N_j} - \left(\frac{M_j}{N_j}\right)^2 = \left(\frac{M_j}{N_j}\right)^2(\xi_j - 1). \quad \text{(A5)}$$

Both methods lead to values of R that approached zero (i.e., the distribution within a bin becomes monodisperse) as the mean mass in a bin approaches a bin boundary; however, the first method predicts values of R smaller than the second for all values of the mean mass. After some experimenting, it is found that the first method tends to sharpen the distribution too rapidly during evaporation, while the second method is overly diffusive, so that taking the average value of R_j yielded better results. In fact, the remapping with this definition of R_j performed better (i.e., it better represented the evolution of the average mass and it is less diffusive) than the old in all off-line tests and is on average three times faster.

[3] Note that the inverse of phase relaxation time, χ, used in the calculation of supersaturation (and implicit in the calculation of τ) goes as $\phi(m)$ integrated over the distribution [i.e., $\chi \approx \langle\phi(m)\rangle$]; consequently, a redefinition of ϕ requires a slight modification of the calculation of the phase relaxation time so that its inverse is no longer exactly proportional to the integral radius.

REFERENCES

Ackerman, A. S., O. B. Toon, and P. V. Hobbs, 1993: Dissipation of marine stratiform clouds and collapse of the marine boundary layer due to depletion of cloud condensation nuclei by clouds. *Science,* **262,** 226–229.

——, ——, and ——, 1994: Reassessing the dependence of cloud condensation nucleus concentration on formation rate. *Nature,* **367,** 445–450.

——, ——, and ——, 1995: A model for particle microphysics, turbulent mixing, and radiative transfer in the stratocumulus-topped marine boundary layer and comparisons with measurements. *J. Atmos. Sci.,* **52,** 1204–1236.

Albrecht, B. A., 1989: Aerosols, cloud microphysics, and fractional cloudiness. *Science,* **245,** 1227–1230.

Austin, P. H., S. Siems, and Y. Wang, 1995: Constraints on droplet growth in radiatively cooled stratocumulus clouds. *J. Geophys. Res.,* **100,** 14 231–14 243.

Baker, M. B., and R. J. Charlson, 1990: Bistability of CCN concentrations and thermodynamics in the cloud-topped boundary layer. *Nature,* **345,** 142–145.

Barkstrom, B. R., 1978: Some effects of 8–12 μm radiant energy transfer on the mass and heat budget of cloud droplets. *J. Atmos. Sci.,* **35,** 665–673.

Belyaev, V. I., 1967: The evolution of the droplet condensation spectrum in clouds. *Izv. Acad. Sci. USSR, Atmos. Oceanic Phys.,* **3,** 341–343.

Betts, A. K., 1973: Non-precipitating cumulus convection and its parameterization. *Quart. J. Roy. Meteor. Soc.,* **99,** 178–196.

Bott, A., T. Trautmann, and W. Zdunkowski, 1995: A microphysical model of the cloud topped marine boundary layer. *Proc. Conf. on Cloud Physics,* Dallas, TX, Amer. Meteor. Soc., 165–170.

Breidenthal, R., 1981: Structure in turbulent mixing layers and wakes using a chemical reaction. *J. Fluid Mech.,* **109,** 1–24.

Broadwell, J. E., and R. E. Breidenthal, 1982: A simple model of mixing and chemical reaction in a turbulent shear layer. *J. Fluid Mech.,* **125,** 397–410.

Brown, P. N., G. D. Byrne, and A. C. Hindmarsh, 1989: VODE: A variable coefficient ODE solver. *SIAM J. Sci. Stat. Comput.,* **10,** 1038–1051.

Charnock, H., 1955: Wind stress on a water surface. *Quart. J. Roy. Meteor. Soc.,* **81,** 639 pp.

Chen, C., and W. R. Cotton, 1983: A one-dimensional simulation of the stratocumulus-capped mixed layer. *Bound.-Layer Meteor.,* **25,** 289–321.

Clark, T. L., 1973: Numerical modeling of the dynamics and microphysics of warm cumulus convection. *J. Atmos. Sci.,* **30,** 857–878.

——, 1974a: A study in cloud phase parameterization using the gamma function. *J. Atmos. Sci.,* **31,** 142–155.

——, 1974b: On modeling nucleation and condensation theory in Eulerian spatial domain. *J. Atmos. Sci.,* **31,** 2099–2117.

——, and W. D. Hall, 1979: A numerical experiment on stochastic condensation theory. *J. Atmos. Sci.,* **36,** 470–483.

Cooper, W. A., 1989: Effects of variable droplet growth histories on droplet size distributions. Part I: Theory. *J. Atmos. Sci.,* **49,** 1301–1311.

Deardorff, J. W., 1970: A numerical study of three-dimensional turbulent channel flow at large Reynolds numbers. *J. Fluid Mech.,* **41,** 453–480.

Egan, B. A., and J. R. Mahoney, 1972: Numerical modeling of advection and diffusion of urban area source pollutant. *J. Appl. Meteor.,* **11,** 312–322.

Feingold, G., B. Stevens, W. R. Cotton, and R. L. Walko, 1994: An explicit cloud microphysics/LES model designed to simulate the Twomey effect. *Atmos. Res.*, **33,** 207–233.

——, ——, ——, and A. R. Frisch, 1996: On the relationship between drop in-cloud residence time and drizzle production in numerically simulated stratocumulus. *J. Atmos. Sci.*, **53,** in press.

Frisch, A. S., C. W. Fairall, and J. B. Snider, 1995: On the measurement of stratus cloud and drizzle parameters with a K_α-band Doppler radar and a microwave radiometer. *J. Atmos. Sci.*, **52,** 2788–2799.

Grabowski, W. W., 1989: Numerical experiments on the dynamics of the cloud-environment interface: Small cumulus in a shear free environment. *J. Atmos. Sci.*, **46,** 3513–3541.

——, and P. K. Smolarkiewicz, 1990: Monotone finite-difference approximations to the advection–condensation problem. *Mon. Wea. Rev.*, **118,** 2082–2097.

Hudson, J. G., and P. R. Frisbie, 1991: Cloud condensation nuclei near marine stratus. *J. Geophys. Res.*, **96,** 20 795–20 808.

Klemp, J. B., and R. B. Wilhelmson, 1978: The simulation of three-dimensional convective storm dynamics. *J. Atmos. Sci.*, **35,** 1070–1096.

Kogan, Y. L., 1991: The simulation of a convective cloud in a 3-D model with explicit microphysics. Part I: Model description and sensitivity experiments. *J. Atmos. Sci.*, **48,** 1160–1189.

——, D. K. Lilly, Z. N. Kogan, and V. V. Filyushkin, 1994: The effect of CCN regeneration on the evolution of stratocumulus cloud layers. *Atmos. Res.*, **33,** 137–150.

——, M. P. Khairoutdinov, D. K. Lilly, Z. N. Kogan, and Qingfu Liu, 1995: Modeling of stratocumulus cloud layers in a large eddy simulation model with explicit microphysics. *J. Atmos. Sci.*, **52,** 2923–2940.

Lilly, D. K., 1962: On the numerical simulation of buoyant convection. *Tellus,* **14,** 148–172.

Liu, Q., Y. L. Kogan, and D. K. Lilly, 1995: Reducing the numerical dispersion of the cloud droplet spectrum in condensation calculations. *Proc., Conf. on Cloud Physics,* Dallas, TX, Amer. Meteor. Soc., 165–170.

Louis, J. F., 1979: A parametric model of vertical eddy fluxes in the atmosphere. *Bound.-Layer Meteor.,* **17,** 187–202.

Martin, G. M., D. W. Johnson, and A. Spice, 1994: The measurement and parameterization of effective radius in warm stratocumulus clouds. *J. Atmos. Sci.*, **51,** 1823–1842.

Mason, P. J., 1994: Large eddy simulations: A critical review of the technique. *Quart. J. Roy. Meteor. Soc.*, **120,** 1–26.

Moeng, C.-H., 1984: A large-eddy-simulation model for the study of planetary boundary layer turbulence. *J. Atmos. Sci.*, **41,** 2052–2062.

——, 1986: Large-eddy simulation of a stratus-topped boundary layer. Part I: Structure and budgets. *J. Atmos. Sci.*, **43,** 2886–2900.

——, and Coauthors, 1995: Simulation of a stratocumulus-topped PBL: Intercomparison among different numerical codes. *Bull. Amer. Meteor. Soc.*, **76,** 261–278.

Nicholls, S., 1984: The dynamics of stratocumulus: Aircraft observations and comparisons with a mixed layer model. *Quart. J. Roy. Meteor. Soc.*, **110,** 783–820.

——, 1989: The structure of radiatively driven convection in stratocumulus. *Quart. J. Roy. Meteor. Soc.*, **115,** 487–511.

Nieuwstadt, F. T. M., P. J. Mason, C-H. Moeng, and U. Schumann, 1991: Large-eddy simulation of the convective boundary layer: A comparison of four computer codes. *Turbulent Shear Flows 8: Selected Papers from the 8th International Symposium on Turbulent Shear Flows.* Springer-Verlag, 405 pp.

Noonkester, V. R., 1984: Droplet spectra observed in marine stratus cloud layers. *J. Atmos. Sci.*, **41,** 829–845.

Pielke, R. A., W. R. Cotton, R. L. Walko, C. J. Tremback, W. A. Lyons, L. D. Grasso, M. E. Nicholls, M. D. Moran, D. A. Wesley, T. J. Lee, and J. H. Copeland, 1992: A comprehensive meteorological modeling system—RAMS. *Meteor. Atmos. Phys.*, **49,** 69–91.

Pincus, R., and M. B. Baker, 1994: Effect of precipitation on the albedo susceptibility of marine boundary layer clouds. *Nature,* **372,** 250–252.

Rooth, C., 1957: On a special aspect of the condensation process and its importance in the treatment of cloud particle growth. *Tellus,* **9,** 372–377.

Sedunov, Y. S., 1965: Fine cloud structure and its role in the formation of the cloud particle spectrum. *Izv. Acad. Sci. USSR, Atmos. Oceanic Phys.*, **1,** 722–731.

Shettle, E. P., and R. W. Fenn, 1979: Models for the aerosols of the lower atmosphere and the effects of humidity variations on their optical properties. Tech. Rep., Air Force Geophysics Laboratory, AFGL-TR-79-0214, 94 pp.

Slingo, A., R. Brown, and C. L. Wrench, 1982: A field study of nocturnal stratocumulus. Part III: High resolution radiative and microphysical observations. *Quart. J. Roy. Meteor. Soc.*, **108,** 145–165.

Smolarkiewicz, P. K., and W. W. Grabowski, 1990: The multidimensional positive definite advection transport algorithm: Nonoscillatory option. *J. Comput. Phys.*, **86,** 355–375.

Squires, P., 1952: The growth of cloud drops by condensation. *Aust. J. Sci. Res.*, **A5,** 59–86.

Stepanov, A. S., 1976: Influence of turbulence on the size spectrum of cloud drops during condensation. *Izv. Acad. Sci. USSR, Atmos. Oceanic Phys.*, **12,** 281–292.

Stevens, B., R. L. Walko, W. R. Cotton, and G. Feingold, 1996: On the spurious production of cloud edge supersaturations by Eulerian models. *Mon. Wea. Rev.*, in press.

Tremback, C. J., J. Powell, W. R. Cotton, and R. A. Pielke, 1987: The forward in time upstream advection scheme: Extension to higher orders. *Mon. Wea. Rev.*, **115,** 540–555.

Tripoli, G. J., and W. R. Cotton, 1981: The use of ice-liquid water potential temperature as a thermodynamic variable in deep atmospheric models. *Mon. Wea. Rev.*, **109,** 1094–1102.

Tzivion, S., G. Feingold, and Z. Levin, 1987: An efficient numerical solution to the stochastic collection equation. *J. Atmos. Sci.*, **44,** 3139–3149.

——, ——, and ——, 1989: The evolution of rain-drop spectra. Part II: Collisional collection/breakup and evaporation in a rain shaft. *J. Atmos. Sci.*, **46,** 3312–3327.

Twomey, S., 1977: The influence of pollution on the shortwave albedo of clouds. *J. Atmos. Sci.*, **34,** 1149–1152.

Zalesak, S. T., 1979: Fully multidimensional flux-corrected transport algorithms for fluids. *J. Comput. Phys.*, **31,** 335–362.